Influence of porosity structures on mixing-induced reactivity at chemical equilibrium in mobile/immobile Multi-Rate Mass Transfer (MRMT) and Multiple INteracting Continua (MINC) models

Jean-Raynald de Dreuzy, Alain Rapaport, Tristan Babey, Jérôme Harmand

▶ **To cite this version:**

Jean-Raynald de Dreuzy, Alain Rapaport, Tristan Babey, Jérôme Harmand. Influence of porosity structures on mixing-induced reactivity at chemical equilibrium in mobile/immobile Multi-Rate Mass Transfer (MRMT) and Multiple INteracting Continua (MINC) models. Water Resources Research, 2013, 49 (12), pp.8511-8530. 10.1002/2013WR013808 . hal-00914049

HAL Id: hal-00914049
https://inria.hal.science/hal-00914049

Submitted on 28 Feb 2014

HAL is a multi-disciplinary open access archive for the deposit and dissemination of scientific research documents, whether they are published or not. The documents may come from teaching and research institutions in France or abroad, or from public or private research centers.

L'archive ouverte pluridisciplinaire **HAL**, est destinée au dépôt et à la diffusion de documents scientifiques de niveau recherche, publiés ou non, émanant des établissements d'enseignement et de recherche français ou étrangers, des laboratoires publics ou privés.

Influence of porosity structures on mixing-induced reactivity at chemical equilibrium in mobile/immobile Multi-Rate Mass Transfer (MRMT) and Multiple INteracting Continua (MINC) models

J.-R. de Dreuzy,[1,2] A. Rapaport,[3,4] T. Babey,[1] and J. Harmand[4,5]

Received 19 March 2013; revised 20 September 2013; accepted 5 November 2013; published 19 December 2013.

[1] Trapping mechanisms and slow diffusion in poorly connected porosities are well modeled by several anomalous transport models including the Multi-Rate Mass Transfer framework (MRMT). In MRMT, solutes in fast mobile advective zones are slowed down by first-order exchanges with immobile zones. While MRMT models have been used essentially for conservative transport, we investigate their relevance to reactive transport. To this end, we analyze the influence of the structure of the diffusive porosity zone on the distribution of concentrations within the immobile zone and on the reactivity of simple precipitation/dissolution bimolecular reactions at equilibrium. We build Multi-Rate Mass Transfer (MRMT) and Multiple INteracting Continua (MINC) models with equivalent transport characteristics. Both models have the same mobile zone concentrations at any time. They, however, differ by the connectivity structure of their immobile zones. MRMT has a star-shaped connectivity structure with the mobile zone linked to all immobile zones and acting as the sole exchanger. MINC has a chained-type connectivity where immobile zones are mutually connected on a line. We show that both connectivity structures give the same concentration variance whatever the model parameters, dimensionality, and initial conditions. Reaction rates of bimolecular reaction at chemical equilibrium are also highly similar but not equal as long as concentration gradients within the diffusive zone remain low like in the uniform injection case, or at large times when high initial concentration gradients have been reduced. For high initial immobile concentration gradients in the diffusive zone, however, reaction rates are much lower in the star-shaped connectivity structure (MRMT), and consequently depend on the organization of the immobile porosity structure. Negative concentrations also occur in some of the immobile zones of the equivalent MRMT as a result of the direct connection of the mobile and immobile zones. While acceptable for conservative components, negative concentrations limit the relevance of MRMT to model reactivity at high immobile concentration gradients. The concept of immobile zone concentration should thus be taken with great care and systematically be assessed.

Citation: de Dreuzy, J.-R., A. Rapaport, T. Babey, and J. Harmand (2013), Influence of porosity structures on mixing-induced reactivity at chemical equilibrium in mobile/immobile Multi-Rate Mass Transfer (MRMT) and Multiple INteracting Continua (MINC) models, *Water Resour. Res.*, *49*, 8511–8530, doi:10.1002/2013WR013808.

1. Introduction

[2] Solute exchanges between high and low-permeability zones are recognized as one of the key factors controlling solute transport in geological media. High-permeability zones promote fast solute transport with a dominance of advection over diffusion while transport is much slower and essentially diffusive in the low-permeability zones. Coexistence of these mobile and immobile zones and exchanges between them critically enhance solute spreading, breakthrough tailing and anomalous non-Fickian transport [*Benson et al*., 2000; *Berkowitz et al*., 2006; *Bouchaud and Georges*, 1990; *Dentz and Berkowitz*, 2003; *Neuman and Tartakovsky*, 2009]. It is widely observed in fractured media where the high-permeability zones are long and highly transmissive fractures while the low-permeability zones are the smaller fractures, the dead ends of the fracture network as well as the surrounding unfractured rock (matrix) [*Andersson et al*., 2004; *Gouze et al*., 2008; *Grisak and Pickens*, 1980; *McKenna et al*., 2001; *Neretnieks*, 1980; *Shapiro*, 2001]. It also prevails in

[1]Géosciences Rennes, UMR CNRS 6118, Campus de Beaulieu, Rennes, France.
[2]Institute of Environmental Analysis and Water Studies, CSIC, Barcelona, Spain.
[3]UMR 729 INRA SupAgro MISTEA, Montpellier, France.
[4]EPI INRA INRIA MODEMIC, Sophia-Antipolis, France.
[5]INRA-LBE, UR 0050, Avenue des étangs, Narbonne, France.

Corresponding author: J.-R. de Dreuzy, Géosciences Rennes, UMR CNRS 6118, Campus de Beaulieu, Université de Rennes 1, FR-35042 Rennes CEDEX, France. (Jean-Raynald.de-Dreuzy@univ-rennes1.fr)

©2013. American Geophysical Union. All Rights Reserved.
0043-1397/13/10.1002/2013WR013808

porous media with high contrasts of lithologies [*Haggerty et al*., 2004; *LeBlanc et al*., 1991; *Sudicky*, 1986], in microscale inclusion models [*Golfier et al*., 2007; *Zinn et al*., 2004] and in radial diffusion in soils [*Rao et al*., 1980; *Wu and Gschwend*, 1986]. In fractured media, solute transport has been based on structure-imitating approaches like fracture-matrix concepts [*Maloszewski and Zuber*, 1985; *Sudicky and Frind*, 1982; *Tang et al*., 1981], Multiple INteracting Continua (MINC) [*Karimi-Fard et al*., 2006; *Pruess and Narasimhan*, 1985] and dual or triple-porosity concepts [*Magnico et al*., 1993; *Wu and Pruess*, 2000; *Wu et al*., 2004]. Regarding inert solute transport, these different approaches can all be accounted within the Multiple-Rate Mass Transfer framework (MRMT) [*Carrera et al*., 1998; *Ginn*, 2009; *Haggerty and Gorelick*, 1995; *Haggerty et al*., 2000; *Willmann et al*., 2008]. MRMT models consist of mobile zones exchanging solutes with several immobile zones according to a first-order exchange law. Despite their simplicity, MRMT models are highly general and can simultaneously model the interaction with different structures of diffusive zones and even different trapping mechanisms (e.g., diffusion in low-flow zones and sorption) [*Haggerty and Gorelick*, 1995].

[3] The equivalence between the MRMT models and the other fracture-matrix types of model is based on the equality of the concentrations in the mobile zone and, consequently, of the solute breakthrough curves [*Haggerty and Gorelick*, 1995]. Fundamentally, the diffusion in 1-D, 2-D, and 3-D inclusions is solved analytically in the Laplace domain, and the analytical solution is decomposed in partial fractions. Each partial fraction is further interpreted as a first-order exchange between the concentration in the mobile zone and an equivalent "virtual concentration" in the immobile zone. When keeping the focus on the transport properties, the important quantity is the concentration in the mobile zone and the status of the immobile "virtual concentrations" does not have to be further considered. However, it becomes a key issue when addressing reactivity in the immobile zone. It is tempting to use these immobile "virtual concentrations" as regular chemical concentrations of solutes that can be handled as concentrations of chemical compounds that can react chemically [*Donado et al*., 2009]. Nothing in the construction of the MRMT however ensures this, hence the term of "virtual concentration." The equivalence of *Haggerty and Gorelick* [1995] does not implicate anything on the distribution of concentrations nor on mixing capacities and reaction rates within the immobile zones. While the flux of concentration between the mobile and immobile zones is fully constrained, the concentration distributions in the immobile zones do not have any reason to be similar.

[4] Intuitively, the immobile concentration distribution does not only depend on the concentration in the mobile zone but also on the topological structure of the immobile zones, which are highly different in the MRMT and in the other approaches. In the multiple-interacting model (MINC), which can be considered as a discretization of the fracture-matrix model [*Pruess and Narasimhan*, 1985; *Pruess*, 1992], the immobile zones are connected in series and linked to the mobile zone by a single immobile zone (Figure 1a). This sketch is correct whatever the dimensionality of the fracture-matrix model (1-D layer, 2-D cylinder, and 3-D spheres) as long as initial conditions do not break their symmetry. For MRMT, all immobile zones are connected in parallel to the mobile zone (Figure 1b). The mobile zone can be seen as a mixer that distributes solutes directly to all immobile zones. For MINC, however, access to the immobile zones depends on their position in the series of the immobile zones. Solute exchange is more remote and critically depends on all the closer immobile zones. Interactions between immobile solute concentrations are expected to be more complex in MINC because of its linear topological structure than in the simpler topology of MRMT.

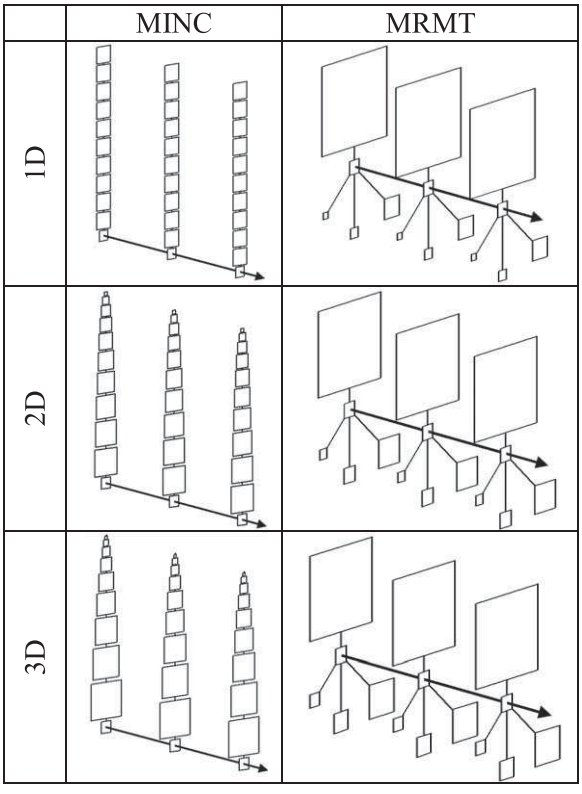

Figure 1. Sketches of the immobile zone organization for Multiple INteracting Continuum models (MINC) and Multiple-Rate Mass Transfer models (MRMT) for 1-D, 2-D, and 3-D inclusions. Mobile zones are identified by the connection arrow and their volume is exaggerated five times compared to the volume ratio taken for the simulation ($\beta = 100$). Comparison with the MRMT model shows the large dominance of the smallest rates having the largest volumes. Impact of the inclusion dimension intervenes in the rate values and on the rate of volume reduction smaller with higher dimensions.

[5] The dynamic of mixing also intuitively depends on the connectivity structure. The potential influence of structure is a priori not limited to the distribution of concentrations in the immobile zones but likely extends to mixing induced reactivity. Mixing can be characterized by the temporal derivative of the second moment of the concentration distribution M_2 [*Le Borgne et al*., 2010]

$$\chi(t) = -\frac{1}{2}\frac{dM_2}{dt}. \quad (1)$$

[6] This quantity defined as the scalar dissipation gives the rate of scalar mixing. As most of the porous volume is in the immobile zones rather than in the mobile zone [*Li et al*., 2011; *Willmann et al*., 2008], their concentration as well the dynamic of their exchanges are likely to impact the concentration variance and hence the reactivity in the absence of any mineralogical heterogeneity [*Glassley et al*., 2002]. In this article, we aim at exploring the influence of the organization of the immobile zones on the mixing characteristics and induced reactivity at chemical equilibrium at identical conservative solute transport.

[7] Previous studies are not answering directly this question as structures are all significantly more complex than the simpler MRMT and MINC configurations. Immobile zone organization is one parameter among others including the heterogeneity of the permeability field and the complexity of the flow structure (mobile zone organization, heterogeneous advection) [*Gramling et al*., 2002; *Luo and Cirpka*, 2008, 2011; *Willmann et al*., 2010]. However, in reaction-transport-diffusion dynamics, it is known that simple spatial structures can induce nonintuitive behaviors worth to be investigated [e.g., *Haidar et al*., 2011]. In this article, we focus on the sole effect of the immobile zone organization on the distribution of the immobile zone concentrations and on the mixing-induced reactivity on the basis of elementary connectivity structures.

2. Models and Methods

[8] We first recall the MRMT and MINC models, express them in dimensionless form and list the methods used to characterize conservative and reactive transport. We then detail the specificities of the numerical experiments including the initial conditions, the simulation parameters, and the computational methods.

2.1. Models

[9] We consider classical MRMT and MINC models that only differ by their immobile zone organization. The total porous volumes of the mobile and immobile zones are identical in both models. Even if they are not limited to diffusion in simple media, both MRMT and MINC models fundamentally derive from two different discretizations of the diffusion equation in homogeneous monodisperse inclusion zones of Euclidean dimension n in interaction with a 1-D mobile zone [*Haggerty and Gorelick*, 1995; *Pruess and Narasimhan*, 1985; *Sudicky and Frind*, 1982; *Tang et al*., 1981]. The fundamental set of equations for the 1-D mobile zone in interaction with diffusion in the immobile zone of dimension n are given in dimensional form

$$\frac{\partial c(x,t)}{\partial t} + \beta\frac{\partial \tilde{s}(x,t)}{\partial t} = -v\frac{\partial c(x,t)}{\partial x} + D_m\frac{\partial^2 c(x,t)}{\partial x^2}, \quad (2)$$

$$\frac{\partial s(x,r,t)}{\partial t} = \frac{d}{r^{n-1}}\frac{\partial}{\partial r}\left(r^{n-1}\frac{\partial s(x,r,t)}{\partial r}\right) \text{for } 0 \le r \le a, \quad (3)$$

$$\tilde{s}(x,t) = \int_0^a s(x,r,t)r^{n-1}dr \Big/ \int_0^a r^{n-1}dr, \quad (4)$$

where $c(x, t)$ is the mobile concentration at the scalar position x along the mobile domain $x \ge 0$, $s(x, r, t)$ is the immobile zone concentration at the microscopic distance r from the mobile zone and at the macroscopic position x, $\tilde{s}$ is the mean concentration in the immobile zone, a is the characteristic scale of the immobile zone (e.g., radius of spherical immobile inclusions in 3-D), v and D_m are the velocity and longitudinal dispersion coefficient in the mobile zone, d is the diffusion coefficient in the immobile zone and β is equal to the ratio of immobile to mobile porous volumes, also equal to the asymptotic repartition of the masses of solutes between the immobile and mobile zones. The concentration in the immobile zone is equal to the concentration of the mobile zone at the interface and no flow is imposed at the boundary $r = 0$

$$s(x, r=a, t) = c(x,t), \quad (5)$$

$$\left.\frac{\partial s}{\partial r}\right|_{r=0} = 0. \quad (6)$$

[10] Initial conditions are imposed in the mobile and immobile zones

$$s(x, r, t=0) = s_0(x,r), \quad (7)$$

$$c(x, t=0) = c_0(x). \quad (8)$$

[11] A dimensionless formulation of the problem can be obtained by choosing as the reference time the characteristic time of diffusion within the immobile zone $\tau = a^2/d$ and as the reference scale the characteristic immobile zone scale a

$$\frac{\partial c}{\partial \bar{t}} + \beta\frac{\partial \tilde{s}}{\partial \bar{t}} = -\frac{va}{d}\frac{\partial c}{\partial \bar{x}} + \frac{D_m}{d}\frac{\partial^2 c}{\partial \bar{x}^2}, \quad (9)$$

$$\frac{\partial s}{\partial \bar{t}} = \frac{1}{\bar{r}^{n-1}}\frac{\partial}{\partial \bar{r}}\left(\bar{r}^{n-1}\frac{\partial s}{\partial \bar{r}}\right) \text{for } 0 \le \bar{r} \le 1, \quad (10)$$

$$\tilde{s} = \int_0^1 s(x,\bar{r},t)\bar{r}^{n-1}d\bar{r} \Big/ \int_0^1 \bar{r}^{n-1}d\bar{r} \quad (11)$$

with $\bar{x} = x/a$, $\bar{r} = r/a$, and $\bar{t} = t/\tau$. The system of equations (9–11) depends on 3-D parameters, the capacity ratio β, the Damköhler number $Da = \frac{va}{d}$ that compares the characteristic diffusion time in the immobile zone with the characteristic advection time in the mobile zone and the ratio $R_d = \frac{D_m}{d}$ that compares the dispersion in the mobile zone and the diffusion in the immobile zone. In the following, R_d will be taken small enough ($R_d = 10^{-3}$) so that the effect of the dispersion in the mobile zone can be neglected as compared to the exchanges with the immobile zone. For convenience, all overbars will also be dropped as everything will be expressed in dimensionless form.

[12] In cases where both MINC and MRMT models result from a discretization of diffusion in 1-D, 2-D, or 3-D inclusions, equations (5–8) subjected to boundary and initial conditions (9–11) can be synthesized as (Appendix A)

$$M\left[\frac{\partial U}{\partial t} - L(RU)\right] = AU, \quad (12)$$

where $U = (\,C \quad S_1 \quad \ldots \quad S_N\,)^T$ is the vector of the mobile and N immobile concentrations $C(x, t)$ and $S_i(x, t)$

$(i=1,\ldots,N)$, where N is the number of immobile zones. Upper case letters are used for discretized quantities transversally to the mobile zone while lower case letters are used for continuous quantities. R is the restriction operator to the mobile zone. All elements of R are zero except for the element on the first row and first column equal to 1. L is the transport operator in the mobile zone

$$L(U)=-Da\frac{\partial U}{\partial x}+R_d\frac{\partial^2 U}{\partial x^2}. \quad (13)$$

[13] M is a diagonal matrix of the porous volumes of the mobile and immobile zones and A is a matrix characterizing their mutual interactions. The volume and interaction matrices M and A are derived for the MINC model and recalled for the MRMT model in Appendix A. Because diffusion is a nondirectional process and as the system of equation (12) is written in terms of solute mass conservation, A is a symmetrical Metzler matrix the sums across columns are equal to zero and all its off-diagonal elements are nonpositive. A characterizes a self-adjoint process.

[14] A is a kind of adjacency matrix weighted by the physical properties of the immobile inclusions [*Godsil and Royle*, 2001]. For MRMT models, A is an "arrow" type matrix where only the first line and the first column have nonzero off-diagonal elements because all the interactions occur between the mobile and immobile zones and none between immobile zones. For MINC models, A is a classical tridiagonal matrix traducing the interactions between neighboring immobile zones. Interaction with the mobile zone is performed only through the immobile zone next to the mobile zone and is expressed by the boundary condition (5).

2.2. Concentration Moments, Mixing Characteristics, and Reaction Rate

[15] We compare equivalent MRMT and MINC models on several different characteristics of the resulting concentration fields beginning first with the mean dimensionless velocity $V=d\langle x\rangle/dt=dm_1/dt$ and the dimensionless dispersion coefficient D with

$$D=\frac{1}{2}\frac{d\sigma_x^2}{dt}, \quad (14)$$

[16] Where

$$\sigma_x^2=m_2/m_0-(m_1/m_0)^2 \quad (15)$$

and the spatial moments m_k are

$$m_k=\int_{x=0}^{\infty}\sum_{i=1}^{N}x^k M(i,i)U_i(x)dx, \quad (16)$$

where we recall that $M(i, i)$ is the volume of the immobile zone i. $\langle x\rangle$ and σ_x^2 should be very close for equivalent MRMT and MINC models. They are not equal because of different discretization errors for the MINC method and truncation errors for the MRMT. Nonetheless, it will be used as a test of consistency of the numerical methods. Tests will be performed on the statistical quantities $\langle x\rangle$ and σ_x^2 rather than on their temporal derivatives V and D to avoid any loss of accuracy due to the derivation.

Table 1. Characteristic Time (α_i^{-1}), Relative Porosity Ratio of the Five First Rates of the MRMT Series for $n = 1$ (b_i) and Cumulative Relative Porosity Ratio of the First Few Rates $\sum_{k=1}^{i} b_k$

i	α_i^{-1}	b_i (%)	$\sum_{k=1}^{i} b_k$ (%)
1	0.4	81	81
2	0.045	9	90
3	0.016	3.3	93.3
4	0.0083	1.65	95
5	0.0050	1	96

[17] The second set of characteristics concerns the distribution of concentrations in the mobile and immobile zones. We build the histogram of the distribution of the decimal logarithm of concentrations ($p(\log C)$). The logarithm of concentrations is a priori more appropriate than the concentration itself because concentrations are expected to be broadly distributed over several orders of magnitude. To get more quantitative information, we compute the moments of the concentration distribution M_k

$$M_k=\int_{x=0}^{\infty}\sum_{i=1}^{N+1}M(i,i)[U_i(x)]^k dx \quad (17)$$

for the first integral values of k (k ranging from 1 to 5) where N is either equal to N_{MRMT} or N_{MINC}. The moments are less sensitive than the distribution itself to the strong dominance of the first rates in the MRMT model that make the distribution more discrete than continuous in the preasymptotic regime. They can also be computed whatever the concentration values.

[18] We shorten the denomination of "immobile zone with the kth rate" by the "kth rate." So the first rate designates the immobile zone with the smallest rate. It is also the immobile zone with the largest volume as the volume is decreasing with the rate. In the layered inclusion case, the first rate counts for 81 % of the total immobile porosity (Table 1). The five first rates count for 96 % of the total immobile porosity. Most of the porosity is thus concentrated in the very few first rates.

[19] The moments of the concentration distribution M_k should not be confused with the spatial moments of the concentration m_k. M_0 is the total porous volume of the domain simulated. M_1 is the mass within the domain. It is constant and expresses the conservation of mass as long as all the mass remains within the domain. As the total mass will be injected at the initial time and will be set at 1 (see section 2.3), M_k is numerically equal to the raw moment of order k and will be assimilated to it. We kept the nonnormalized equation (17) for M_k to systematically check that the total mass M_1 remains constant and equal to 1. Higher-order moments ($k>1$) are nonlinear outputs of a linear model. M_2 gives an indication of the mixing-induced reactivity as it is linked to the scalar dissipation rate $\chi(t)$ by equation (1). We finally compute the reaction rate of a

bimolecular dissolution/precipitation reaction at chemical equilibrium from the concentration field of a conservative component. We assume the same diffusion coefficient for the two reactants, what might not be always the case [*Hochstetler et al*., 2013]. If A and B are the reactants and C_A and C_B their concentration vectors in the mobile and immobile zones, the conservative component $U = C_A - C_B$ follows equation (12) while the reaction rate R_C can be expressed by

$$R_C(t) = \int_{x=0}^{\infty} \sum_{i=1}^{N+1} R_{Ci}(x,t)dx \tag{18}$$

with

$$R_{Ci}(x,t) = M\left[\frac{\partial C_{Ai}(x,t)}{\partial t} - L(RC_{Ai}(x,t))\right] - AC_{Ai}(x,t) \tag{19}$$

and $C_{Ai}(x,t) = \frac{U_i(x,t)+\sqrt{U_i(x,t)^2+4K}}{2}$ where $C_{Ai}(x,t)\, C_{Bi}(x,t) = K$ for $i = 1, \ldots, N+1$ [*de Simoni et al*., 2005; *Rubin*, 1983]. K is the chemical equilibrium constant. The precipitated/dissolved mineral is assumed to have an activity equal to 1 and thus does not show up in the equations. To avoid any additional temporal derivative error, the derivative of C_A is directly determined from the derivative of the conservative component U rather than recomputed

$$\frac{\partial C_A}{\partial t} = \frac{\partial C_A}{\partial U}\frac{\partial U}{\partial t}. \tag{20}$$

[20] The reaction rate of equation (19) will be derived using the concentration of A and its derivative given by equation (20). Reactant concentrations are equal at equilibrium in most of the domain $C_{Ai} = C_{Bi} = \sqrt{K}$ corresponding to a zero value of the conservative component U_i ($U_i = 0$), outside of the narrow injection zone where the difference of their concentrations is strictly positive ($U_i > 0$). We derive the reaction rates in both MINC and MRMT models with this simple initial condition under the assumptions that the two species A and B are always present and that no kinetic reactions interfere with their activities [*Donado et al*., 2009]. In the case of the diffusion model, the reaction rate can be expressed as the product of a chemical and a physical factor [*de Simoni et al*., 2005]

$$R_{Ci} = \frac{\partial^2 C_{Ai}}{\partial U_i^2} \nabla^T U_i d_G \nabla U_i, \tag{21}$$

where $d_G = 1$ in the immobile zone ($i = 1$) and $d_G = R_d$ in the immobile zone ($i > 1$). The first chemical term can be simply expressed as

$$\frac{\partial^2 C_{Ai}}{\partial U_i^2} = \frac{2K}{(U_i^2+4K)^{3/2}}, \tag{22}$$

while the second physical factor integrated over the full domain is the scalar dissipation rate $\chi(t)$ related to the derivative of the integral of the squared concentration of the conservative component M_2 by equation (1). The reaction rate thus does not only depend on the M_2 value of the conservative component but also on the higher-order moments of the concentration distribution. Even if we distinguish physical and chemical factors in the reaction rate, all the reactivity remains physically driven by mixing processes of solutes with different concentrations.

2.3. Injection Conditions

[21] To model initial continuous concentration profiles with potentially large gradients, initial concentrations follow a Gaussian profile along the mobile zone centered at the position x_0 sufficiently distant from the system inflow to prevent any spurious boundary effect from the upstream boundary conditions

$$c(x, t=0) = c_0(x) = \frac{1}{\sigma_0\sqrt{2\pi}} e^{-\frac{(x-x_0)}{2\sigma_0^2}}. \tag{23}$$

[22] The standard deviation of the Gaussian is fixed at σ_0 and is five times larger than the initial discretization step. Under these initial conditions, concentrations are normalized so that the total mass injected in the system is equal to 1. For the initial concentrations in the immobile zone, we consider two cases. In the first uniform case, concentrations in the immobile zones are all equal to the concentration in the mobile zone at the same position x

$$s(x, r, t=0) = c(x, t=0). \tag{24}$$

[23] The initial ratio of mass in the mobile and immobile zones is equal to the capacity ratio β and hardly evolves throughout the simulation. The mean velocity remains also constant. The concentration gradients are initially zero in the immobile zone and are later solely induced by the transport in the mobile zone. We also consider a second case with nonuniform initial concentrations in the immobile zone that highlight the mixing mechanisms. The concentration of the reactant (A) is much larger than the concentration of the other reactant (B) away from the mobile zone. Such cases occur for example when young waters percolate within deeper formations of resident water of composition determined by long-term water-rock interactions [*Aquilina et al*., 2011; *Aquilina and de Dreuzy*, 2011; *Fourcade et al*., 2007; *Techer et al*., 2012].

[24] Concentrations of the conservative component are distributed along the immobile zone according to a uniform profile $g(r)$ in the whole domain

$$s(x, r, t=0) = g(r)c(x, t=0). \tag{25}$$

[25] The profile $g(r)$ is chosen in such a way that the ratio of mass in the immobile and mobile zones remains equal to the capacity ratio so that the velocity remains as close as possible to its asymptotic; F_s value

$$\frac{\int_{r=0}^{r=1} s(x, r, t=0)g(r)dr}{\int_{r=0}^{r=1} g(r)dr} = \frac{c(x, t=0)}{\beta}. \tag{26}$$

[26] We will use this second type of conditions only for $n = 1$, a case for which we derive simple analytical

Table 2. Simulation Parameters Used in Sections 3 and 4[a]

Name	Description	Section 3	Section 4
β	Ratio of immobile to mobile porous volumes	10^2	10^2
D_a	Characteristic diffusion time in the immobile zone to advection time in the mobile zone	10^2	10, 10^2, 10^3
R_d	Ratio of diffusion in the mobile and immobile zones	10^{-3}	10^{-3}
n	Euclidean dimension of immobile zones	1, 2, 3	2
N_{MRMT}	Truncation order in MRMT model	20, 40	20
N_{MINC}	Discretization order in MINC model	20, 40	20
σ_0	Characteristic extension of the initial conditions along the mobile zone	0.1	0.1
Δ_0	Characteristic extension of the initial conditions along to the immobile zone	0.2	0.2
$\overline{K}$	Chemical equilibrium constant	10^{-2}	10^{-1}

[a]Parameters different in section 4 from section 3 are highlighted in bold.

relations between the initial immobile concentrations in the MRMT and MINC frameworks (Appendix B). In this case, we consider a Gaussian profile such as

$$g(r)=\frac{1}{\Delta_0\sqrt{2\pi}}e^{-\frac{r^2}{2\Delta_0^2}}\ \ 0\le r\le\Delta_0 \qquad (27)$$
$$g(r)=0\ \ \Delta_0<r<1.$$

[27] The maximum initial concentration value $u^0_{\max}$ depends on the injection shape and is either

$$u^0_{\max}=\frac{1}{\sigma_0\sqrt{2\pi}} \qquad (28)$$

in the uniform case or

$$u^0_{\max}\approx\frac{1}{\sigma_0\Delta_0\pi} \qquad (29)$$

in the distributed case if Δ_0 is much smaller than 1. The magnitude of the initial concentration is important when considering reactivity as the chemical factor intervening in the reaction rate (equation (22)) depends both on the magnitude of the concentration u and on the equilibrium constant K. Initially, the influence of concentration is dominant over K if

$$u^0_{\max}\gg\sqrt{2K}. \qquad (30)$$

[28] Thus, the ratio $\overline{K}=K/(u^0_{\max})^2$ is a key control parameter of reactivity. If it is very high, reactivity will be exclusively controlled by the scalar dissipation rate with an almost uniform chemical factor. If it is very low, the chemical factor can be highly variable and control reactivity as well as the physical factor.

2.4. Simulation Parameters

[29] We have performed simulations with the following set of common parameters: $\beta=100$, $N_{MINC}=N_{MRMT}=20$. The discretization of the MINC model (N_{MINC}) as well as the truncation of the MRMT model (N_{MRMT}) have a minor influence as long as they are high enough as will be shown in section 3.2. N_{MINC} and N_{MRMT} are more numerical parameters than controlling physical parameters. As a result, the key parameters are the Damköhler number (Da) that compares the characteristic diffusion time in the immobile zone and the characteristic advection time in the mobile zone and the capacity ratio β that characterizes the relative proportion of the immobile to the mobile porous volumes. The influence of the immobile zones increases both with β and Da. Larger β values reduce the velocity and larger Da enhances the global dispersion. In sections 3 and 4, we will investigate the effect of the inclusion dimensionality n ($n=1$, 2, and 3) and of the Damköhler number ($Da=10$, 10^2, and 10^3).

[30] Initial conditions (23–29) are taken with $\sigma_0=0.1$ and $\Delta_0=0.2$. The maximum initial concentration $u^0_{\max}$ is close to either 4 for uniform injection conditions or 15 for distributed injection conditions. The dimensionless equilibrium constant $\overline{K}$ is set at small values of 10^{-2} and 10^{-1} to highlight the possible impact of the concentration variations. All parameter values for sections 3 and 4 are synthesized in Table 2.

2.5. Transport Simulation Methods

[31] Numerous numerical methods have been developed for MRMT and MINC models that either preserve mass [*Başağaoğlu et al*., 2002] or improve precision [*Willmann et al*., 2008]. Here we have chosen a time and space-adaptive method that preserves mass to make simulations over a broad range of temporal scales. For the diffusion model in the immobile zones, the system of equations (10) and (11) with boundary conditions (5) and (6) and initial conditions (8) are discretized with a finite difference scheme as shown in Appendix A. The advection-diffusion equation (9) is handled as the noniterative sequential coupling of the diffusive operator simulated with a finite-difference discretization and of the advective operator simulated with a Lagrangian method. The mobile and immobile methods are sequentially coupled. Temporal integration is performed with an implicit scheme. To simulate transport on a large range of temporal and spatial scales, we use a simple time control method that increases consistently the temporal and spatial steps when the coarse and fine solutions are sufficiently close. The coarsening condition is based on the squared difference of the concentrations divided by the maximal concentration. When it is smaller than a threshold value (10^{-7}), the temporal and spatial steps are simultaneously increased. This method is much faster and almost as accurate as a more classical fully coupled constant time-step Eulerian scheme because of the amplitude of the diffusion induced by the exchanges between the mobile and immobile zones. We have compared it with a more classical Galerkin finite element

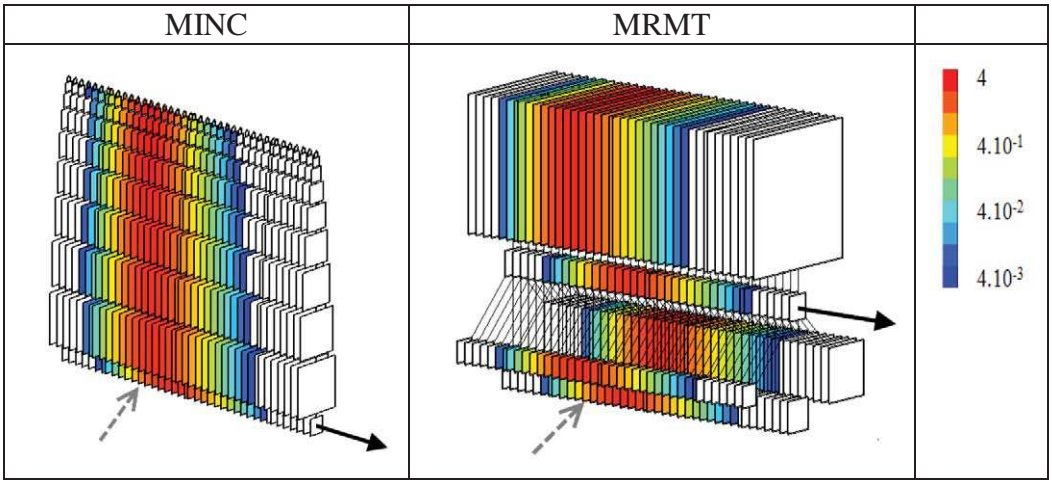

Figure 2. Logarithm of concentration fields in the mobile and 3-D immobile zones with $\beta = 100$ at $t = 0.1$ on 1.5 spatial units for equivalent MINC and MRMT models under uniform injection conditions centered at the location pointed out by the gray arrow. Representation of system structure follows the one given in Figure 1.

method in the mobile zone [*Daus et al*., 1985] fully coupled to the immobile zone for the set of the parameters of section 3 given by Table 2 under uniform initial conditions. Integration of the resulting system of ordinary differential equation was performed with the fourth-order Runge-Kutta method implemented in the ode45 function of MATLAB with the default tolerance values. Both methods lead to the same dispersion, moment and reaction rate results within a relative difference of at most 10^{-3} %. Actual behavior of immobile porous structures with MINC diffusion and equilibrium reactions among the reactants may also be simulated with coarse representation of transport but with realistic chemical reaction(s) in PhreeqC using the MIX and EQUILIBRIUM_PHASES functionalities [*Charlton and Parkhurst*, 2011; *Parkhurst and Appelo*, 1999].

3. Results

[32] Dispersion, concentration moments, and reaction rates are systematically compared as a function of the immobile zone dimensionality under uniform and nonuniform injection conditions both qualitatively and quantitatively.

3.1. Influence of Inclusion Dimensionality Under Uniform Injection Conditions

[33] We first simulate transport starting with classical uniform injection conditions in the mobile and immobile zones (equations (24) and (25)). Exchanges between mobile and immobile zones quickly spread out the concentrations downstream even at one-tenth of the characteristic diffusion time ($t = 0.1$) (Figure 2). Concentrations are broadly distributed over several orders of magnitude. Both MINC and MRMT models display qualitatively the same concentration patterns despite their different connectivity structure.

[34] With these initial conditions, dispersion sharply increases because of the quickly progressing concentration in the mobile zone and because of the trailing concentration trapped in the immobile zone (Figure 3a). About the characteristic dimensionless diffusion time in the immobile zone ($t = 1$), it reaches its asymptotic value D_A. In the asymptotic regime, dispersion fully controls the M_2 value of the concentration field [*de Dreuzy et al*., 2012a; *Le Borgne et al*., 2010]. The larger dimensions induce a faster decrease of the concentration second moment, i.e., the reverse tendency to the asymptotic regime. A crossover occurs before $\bar{t} = 1$. Initially, it is the largest surface to volume ratio for the spherical inclusions that promotes more mixing and faster decrease of M_2. Eventually, it is the largest volume to surface ratio of the layered inclusions that promotes more mixing.

[35] The overall behavior of the reaction rate R_c is more complex than M_2 (Figure 3c). It first slightly increases before steeply decreasing. The increasing trend comes from the chemical factor (equation (22)) while the decreasing trend comes from the physical factor (equation (21)). In fact the chemical factor monotonously increases because the reaction will be highest for equal concentrations of reactants ($U_i = 0$). However, the physical factor monotonously decreases because it is a function of the concentration gradients constantly reduced by the diffusion processes. At first, the increase of the chemical factor dominates the decrease of the physical factor, while, at larger times ($t > 0.1$), the system behavior is dominated by the decrease of the physical factor. In fact, at late times, the reaction rate is directly proportional to the scalar dissipation rate (inset of Figure 3c) as the chemical factor (equation (22)) becomes uniform for values of the conservative component concentration U_i much smaller than $\sqrt{2K}$. Especially, the reaction rate increases with the Euclidean dimension because of the larger surface to volume ratio. At smaller times, the interplay between the chemical and physical factors of reactivity induces several inversions of tendencies of the effect of inclusion dimensionality. At early times, the increase of dimensionality reduces the reaction rate as opposed to what occurs at later times. Reaction rates depend thus not only on M_2 but also on higher-order moments of the concentration distribution.

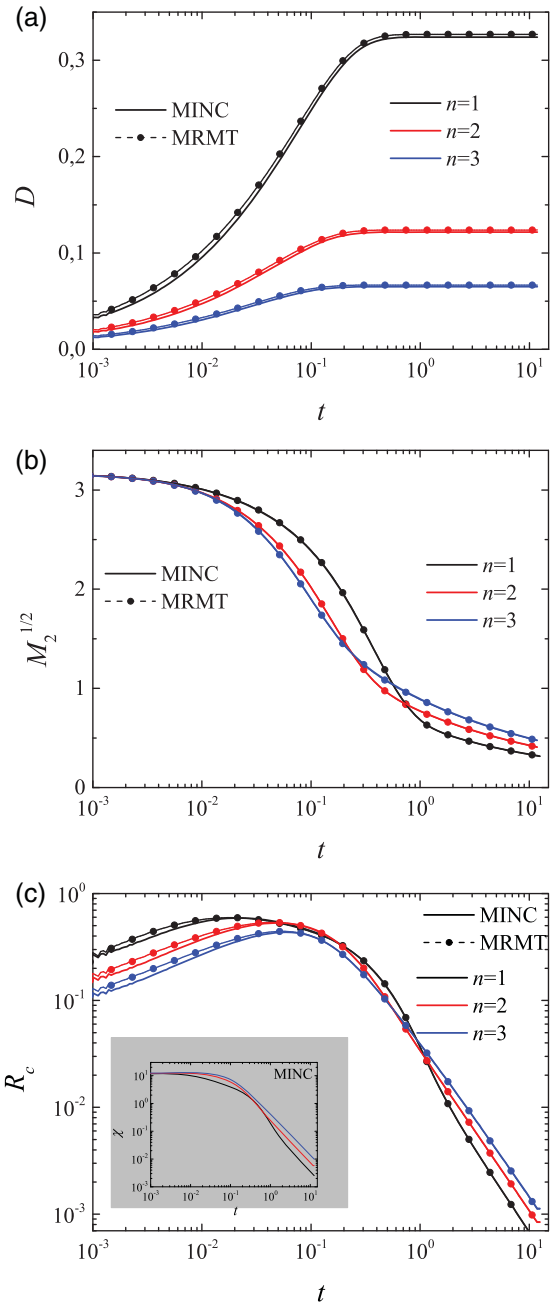

Figure 3. Evolution for equivalent MRMT and MINC models of (a) the dispersion coefficient D, (b) the square root of the second moment concentration moments $M_2^{1/2}$, and (c) the reaction rate R_c and in the gray insert the scalar dissipation rate χ with an initial Gaussian concentration profile uniform in the mobile and immobile zones (n = 1, $Pe = 100$, $\beta = 100$, $R_d = 10^{-3}$, $N = N_{MRMT} = N_{MINC} = 20$).

[36] In fact, $M_k^{1/k}$ display differing temporal evolutions as a function of k (Figure 4). Their initial value $M_k(t{=}0)$ depends on the characteristic width of the injection σ_0

$$M_k(t{=}0) = {\sigma_0}^{1-k}. \tag{31}$$

[37] M_1 remains constant equal to 1 because of mass conservation while the higher-order moments monotonically decrease (Figure 4). The decrease is very sharp between 0.1 and 1 while the concentrations initially trapped in the immobile zone are progressively released in the mobile zone and spread back in the downstream immobile zones. An asymptotic decreasing tendency is reached for $t = 1$. The relative magnitude of the $M_k^{1/k}$ values is reversed around $t = 1$. Around $t = 1$, $M_k^{1/k}$ almost all intersect together. Their asymptotic behavior becomes close when increasing the order k. While the first moments are very close together, concentration distributions are not equal as shown in Figure 5. They differ mostly at intermediary times (Figure 5b, $t = 0.1$) when the dispersion coefficient is steeply increasing. MINC has higher probabilities for the extremes of the distribution. At much earlier and later times (Figures 5a and 5c, $t = 0.025$ and $t = 0.8$), distributions become closer together. High frequency variations of the distribution for the MRMT case come from the quantified volumes of the immobile zones.

[38] The spatial distribution of the reaction rates $R_{Ci}(x, t)$ integrated over time also shows the proximity of the reactivities between MRMT and MINC models (Figure 3). Reactivity sharply decreases downgradient of the injection zone following the reduction of the concentrations and concentration gradients. Reactivity is also more correlated to the volume of the immobile zone rather than to the distance to the immobile zone in MINC or to the reaction rate in MRMT. We note that the reactivities in the mobile zone are not equal as they depend both on the concentrations in the mobile zone and on their relation to the concentrations in the immobile zone (equation (19)). Despite nonobvious relations between reaction rates in the immobile zones for the MRMT and MINC models, the overall variations of the reactivity patterns remain visually very close together.

3.2. Comparison of MRMT and MINC Models

[39] Quite surprisingly, all previously studied quantities remain very close between MRMT and MINC models (Figure 3, lines compared to dots). More quantitatively, we evaluate their relative differences by computing

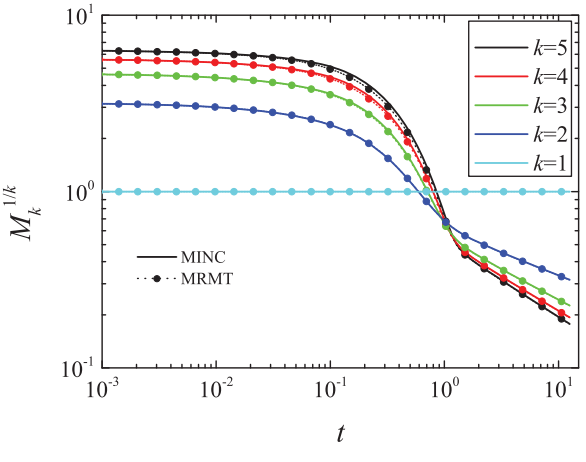

Figure 4. Time evolution of the first five moments of the concentration distribution $M_k^{1/k}$ for the layered case (n = 1) (equation (13)).

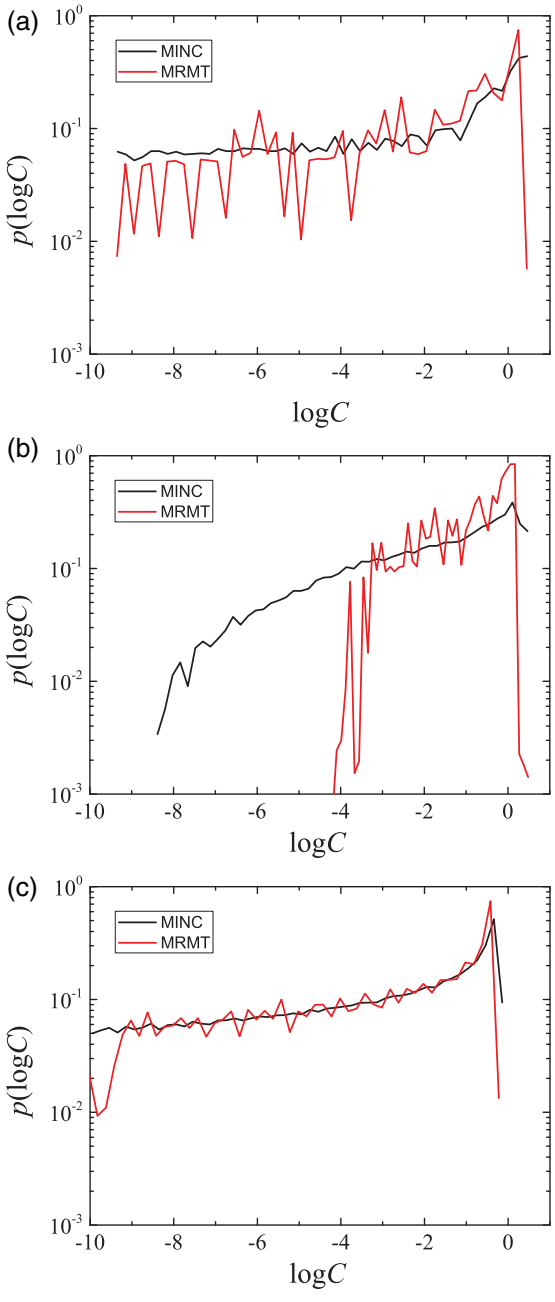

Figure 5. Distribution of the decimal logarithm of concentrations of the mobile and immobile zones at three evolving times $t = 2.5 \times 10^{-2}$, 0.1 and 0.8 for uniform injection conditions.

$$diff(X) = \sqrt{\sum_{i_t=1}^{i_t=n_t} \left[\frac{X^{MINC}(i_t) - X^{MRMT}(i_t)}{(X^{MINC}(i_t) + X^{MRMT}(i_t))/2} \right]^2}, \qquad (32)$$

where X is successively σ_x, $M_k{}^{1/k}$, and R_c (Table 3). While small, differences remain much larger than the estimated numerical accuracy of 10^{-3}%. All quantities are very close whatever the dimensionality of the immobile zone (layered inclusions for $n = 1$, cylindrical inclusions for $n = 2$ and spherical inclusions for $n = 3$). Dispersion values (σ_x) are theoretically equal in both models. Their slight differences decrease with the discretization of the immobile zones. For $N = N_{MRMT} = N_{MINC} = 20$, the mean squared difference is around 1.5%. A refinement of the discretization by a factor of 2 to $N = 40$ reduces the dispersion difference by a factor of around 1.75 to 0.8% − 0.87% (Table 3). Differences in the integrals $M_k{}^{1/k}$ are also small with a maximum at 2.6% and increase with the order k. For $M_2{}^{1/2}$, differences are <0.4% and are reduced by a factor of 2 when refining the immobile zone discretization. For the higher-order moments, differences are not modified by the refined discretization. The M_2 values converge in the MRMT and MINC models while the higher-order integrals slightly differ. They differ by around 0.6% for $M_3{}^{1/3}$, 1.5% for $M_4{}^{1/4}$, and 2.2% for $M_5{}^{1/5}$. Distributions of concentrations are thus not equal but highly close. As a consequence, differences in reaction rates R_c remain small between 2.4% and 5.1% and do not decrease with N as illustrated by the cumulative reaction rates in Figure 6. Differences in reaction rates for the bimolecular reaction are considered to come from the chemical factor rather than from the scalar dissipation rate and the concentration second moment M_2. Because the reaction rate is the product of a physical factor by a chemical factor, the reaction rate depends not only on the scalar dissipation rate but also on higher-order moments of the concentration distribution. Differences in reaction rate depend on the reactivity type and may be larger for more complex reactions.

3.3. Nonuniform Injection Conditions ($n = 1$, Layered Inclusions)

[40] To highlight the possible differences between the concentration distributions and the compensation mechanism within the MRMT model, we analyze the full mobile/immobile problem with nonuniform initial concentrations within the immobile zone described by equations (25–27). Compared to uniform initial conditions, nonuniform initial conditions with injections in the mobile zone and in the remote immobile zone have been chosen to underline possible mixing between immobile concentrations far from the

Table 3. Temporally Integrated Differences $diff(X)$ Between Equivalent MRMT and MINC Models as Defined by Equation (32) for Two Levels of Discretization of the Immobile Zones ($N = N_{MRMT} = N_{MINC}$) Equal to 20 and 40

	n	$diff(\sigma_x)$	$diff(M_2{}^{1/2})$	$diff(M_3{}^{1/3})$	$diff(M_4{}^{1/4})$	$diff(M_5{}^{1/5})$	$diff(R_c)$
$N = 20$	1	0.014	9×10^{-4}	7.8×10^{-3}	0.017	0.026	0.11
	2	0.015	2.5×10^{-3}	6.6×10^{-3}	0.016	0.025	0.090
	3	0.015	4.3×10^{-3}	6.8×10^{-3}	0.011	0.018	0.080
$N = 40$	1	8.0×10^{-3}	4.2×10^{-4}	7.0×10^{-3}	0.016	0.024	0.10
	2	8.5×10^{-3}	1.3×10^{-3}	6.3×10^{-3}	0.016	0.025	0.087
	3	8.7×10^{-3}	2.4×10^{-3}	4.8×10^{-3}	0.01	0.017	0.081

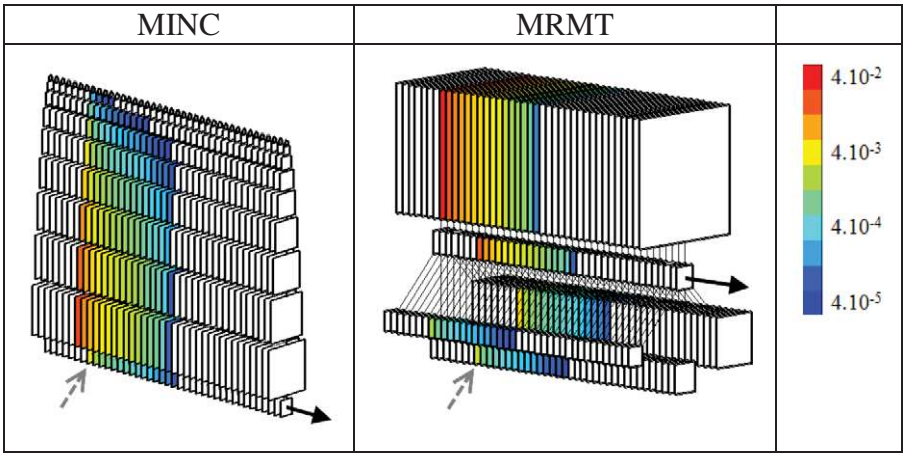

Figure 6. Reactivity integrated between $t = 0$ and $t = 10$. Parameters correspond to those of Figure 2, but with a spatial extension of 30 units.

mobile zone and mobile concentrations. Other parameters are identical to those of the previous section and given in Table 2.

[41] To maintain the comparison between the MINC and MRMT models, the relations between initial conditions in both of these frameworks are developed in Appendix B on the basis of the analytical solution obtained by the separation of variables method. As discussed in Appendix B, some of the initial "virtual concentrations" in the equivalent MRMT model can be negative depending on the shape of the initial conditions in the diffusion model. It is indeed the case for the nonuniform injection conditions as shown by Figure 9. We underline that these negative "virtual concentrations" cannot be considered as numerical errors as they fundamentally come from the sinusoidal function of equation (B3).

[42] The occurrence of the negative "virtual concentrations" in MRMT can be explained in relation to their MINC counterpart. In MINC, the immobile zones void of any concentration between the mobile zone and the remote immobile zones of nonzero concentration act as a "buffer" that must be invaded before the immobile concentration feeds the mobile zone. This lag time is natural in the MINC model where the topology of the connections delays the diffusion of the remote initial immobile concentrations to the mobile zone. In the MRMT model however, all immobile zones start to exchange concentrations at once. To maintain the equivalence between the MRMT and MINC models, the MRMT model introduces negative "virtual concentrations" that offset the contribution of the rates with positive initial concentrations. Initially, successive MRMT zones have opposite signs and the compensation mechanism of the positive and negative incoming "virtual concentrations" in the mobile zone extend over all the immobile zones (Figure 9, black dashed line and disks). The negative "virtual concentrations" progressively vanish as the immobile "virtual concentrations" break through to the mobile zone (Figure 9, solid lines). At $t = 1$, the concentration has broken through to the mobile zone in the MINC model (Figure 9, solid green line) and there is only one negative "virtual concentration" left in the MRMT model (Figure 9, dashed green line and disks). At that same time, almost all of the immobile MRMT zones but the two first ones have uniform concentrations already in equilibrium with the mobile zone because of their high exchange rate.

[43] It should be noted that the negative "virtual concentrations" show up in quite specific cases. They would not occur with uniform injections at any time of the simulation. In fact immobile concentration profiles decreasing from the mobile zone always lead to positive "virtual concentrations" in the MRMT immobile zones (Appendix B). Flat concentration profiles typical of those observed in the retreating concentration from the immobile zone after an initial invasion from the mobile zone also lead to positive concentrations in the MRMT model. In fact, no immobile zone "virtual concentration" can become negative with positive surrounding concentrations because all off-diagonal coefficients of the matrix A of equation (12) are positive or null. The negative "virtual concentrations" thus concern only the injection zone, i.e., the zone where initial concentrations in the immobile zone are nonzero.

[44] Nonetheless the existence of negative "virtual concentrations" induced by the nonuniform injection conditions, dispersions remain very close together in both the MRMT and MINC models (Figure 10a) as well as the second moment of the concentration distribution (Figure 10b) as in the uniform injection case. At later times, the same behavior as for uniform initial conditions is recovered. Reaction rates however strongly differ at early times (i.e., for $t < 0.5$), when concentrations are still influenced by the initial conditions. Differences in reaction rates (Figure 10c) are simultaneous to differences in the high order moments of the concentration distribution $M_k^{1/k}$ $(k > 2)$ (Figure 11). Like in the diffusive flush of the layered inclusion (section 1.1), the distribution of concentrations is narrower in the MRMT case than in the MINC case with a dominance of the concentrations of the smaller rates as shown by the moments of the concentration distribution for $k > 2$ (Figure 11). Even though these concentrations are smaller than the maximal concentrations of the MINC models (Figure 9), their contribution strongly determines the chemical factor of the reaction rate (equation (22)) and leads to 10 times smaller values than in the MINC case (Figure 10c).

[45] Despite the existence of negative "virtual concentrations," the MRMT model is still highly close to the

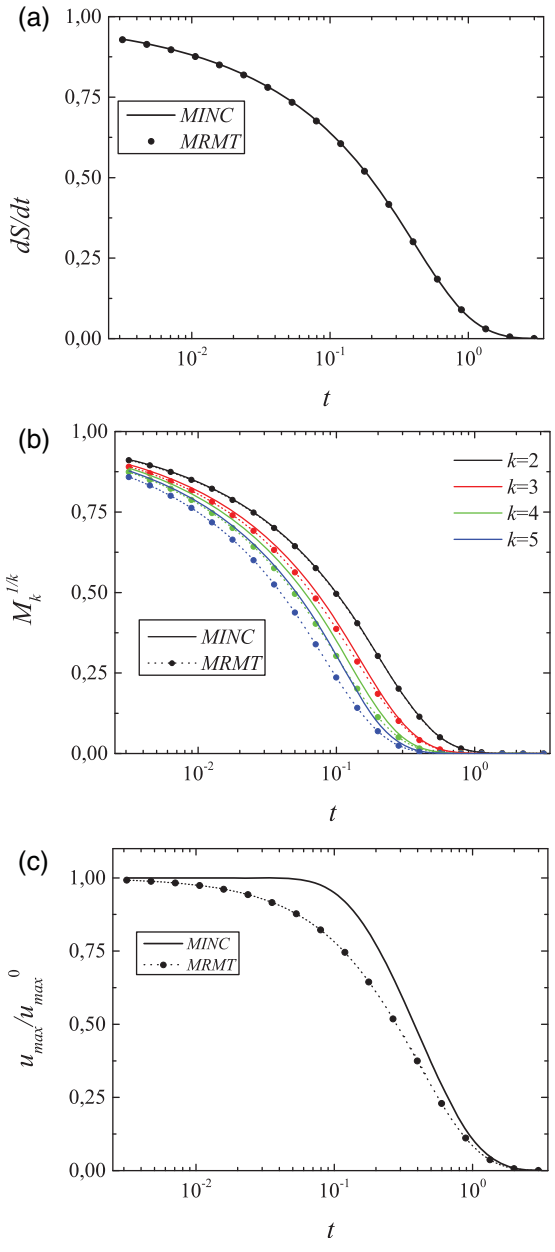

Figure 7. Temporal evolution of (a) the total concentration variation in the immobile zone dS/dt, (b) the $M_k^{1/k}$ for k = 2, . . ., 5, and (c) the maximum concentration u_{max} normalized by its initial value u_{max}^0 for equivalent MRMT and MINC models in the diffusive flush of a 1-D immobile zone.

diffusion model for the dispersion and the second moment of the concentration distribution M_2. The other characteristics (reaction rates and higher-order integrals) however largely differ at early times when the influence of the initial conditions remain nonnegligible. At later times, MRMT and MINC models are again almost equivalent from all respects like in the uniform injection case.

4. Discussion

[46] We discuss successively the conservation of the concentration variance between MRMT and MINC models, the relevance of MRMT models to chemical reactivity, and the influence of the immobile porosity structure on reactivity.

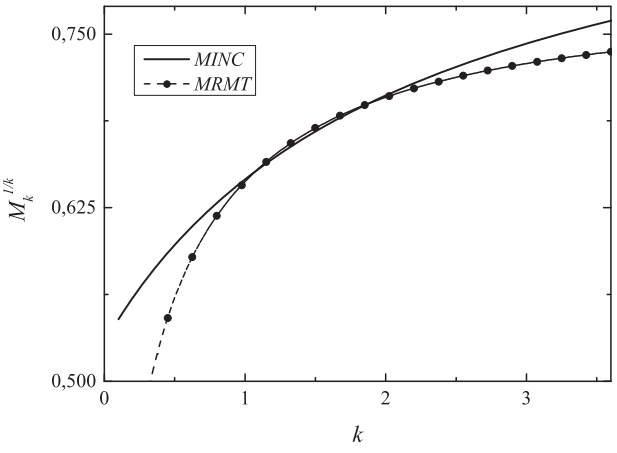

Figure 8. $M_k^{1/k}$ as a function of k for t = 0.1 in the diffusive flush of a 1-D immobile zone.

4.1. Equivalence of Concentration Variance and Scalar Dissipation Rate

[47] The equivalence of the MRMT and MINC models for the second moment of the concentration distribution, a nonlinear output of the linear transport process, was not expected. It can be analytically proven only for layered inclusions ($n = 1$) (Appendix D). The equivalence is hardly affected by the discretization and truncation orders of the MINC and MRMT models as shown by Table 3 as long as the discretization is not too small. We have also checked that the results of the previous section are general and do not depend on the main dimensionless parameters of the model (Da, β, R_d, $\overline{K}$, σ_0, Δ_0) (Table 2). While the influence of these parameters is critical on the outputs observed, the equivalence is not modified. We illustrate this by analyzing systems at different Damköhler number values Da (10, 10^2, 10^3) with other parameters fixed at their values given by Table 2 for $n = 2$ (Figure 12). Larger Da values enhance

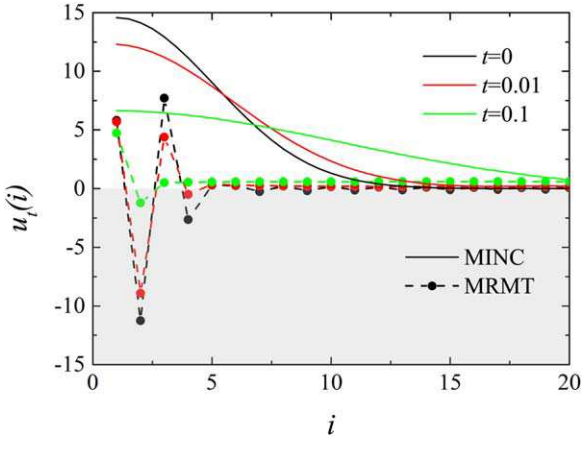

Figure 9. Concentration profiles in the immobile zone for the MRMT and MINC models at initial time ($t = 0$) and at time $t = 0.1$ for the nonuniform injection case. The gray zone underlines the negative concentration area.

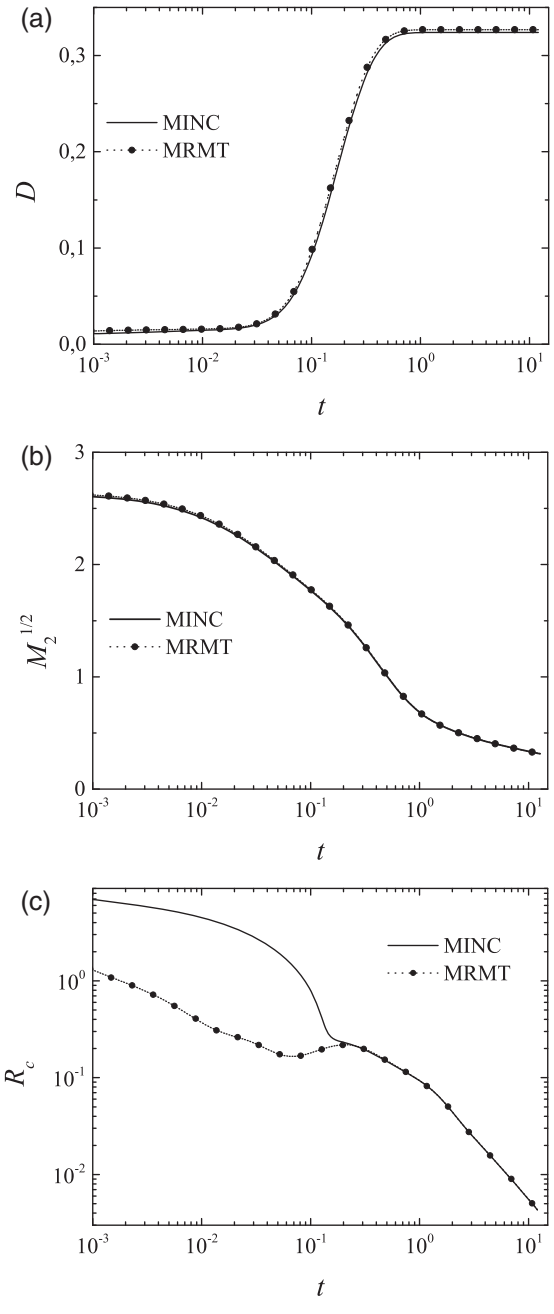

Figure 10. Same as Figure 3 for the nonuniform injection conditions along the immobile zone described by equations (25), (26), and (27). Parameters are given in Table 2, column section 3.

dispersion, mixing and initial reactivity, but do not change the equivalence between MINC and MRMT models.

[48] The equivalence of the second moment of the concentration distribution M_2 is robust as it holds whatever the model parameters, whatever the inclusion dimensionality and for different initial conditions. As M_2 is directly linked to the scalar dissipation rate (equation (1)), MRMT models do not only give consistent breakthrough curves but also consistent concentration variances and scalar dissipation rates. By itself, this result is important as it reinforces the relevance of MRMT models for modeling more complex systems. MRMT models are increasingly used for modeling large-scale transport in heterogeneous media [*Fernandez-Garcia et al.*, 2009; *Li et al.*, 2011; *Willmann et al.*, 2008] and their relevance to inert transport might be generically extended to at least some mixing characteristics like the scalar dissipation rate.

4.2. Relevance of Immobile Concentrations for Chemical Reactions in MRMT Models

[49] The previous analysis shows that the concentration distributions coming from MRMT and MINC models are close together for uniform injection conditions. What we have called in introduction the "virtual concentrations" can be handled as effective chemical concentrations of elements that can react with other elements. It was not granted from the onset, as the "virtual concentrations" are a byproduct of the derivation of the MRMT model from the analytical solutions of the diffusion equation in inclusions of different dimensionalities. In more complex cases however, the relevance of the "virtual concentrations" for reactivity is limited by several factors. The strict equivalence of MRMT and MINC models ends up at the scalar dissipation rate. Both models have different higher-order concentration moments $M_k^{1/k}$ (equation (17)) and different reaction rates (equation (18)) for simple bimolecular reactions at chemical equilibrium. If differences remain small (of the order of a few percents) for uniform injection conditions along the immobile zone, differences can be quite large with nonuniform injection conditions in the time range where the influence of the initial conditions remains nonnegligible. It is especially the case when initial conditions are nonzero far from the mobile zone.

[50] The largest differences come from the initial negative "virtual concentrations" of some of the MRMT rates in the nonuniform injection case. These negative "virtual concentrations" are necessary to ensure the initial delay of the concentration breakthrough to the mobile zone. They could be acceptable for conservative components. In the case of the bimolecular reaction previously described, positive and negative concentrations would correspond to one of the reactant concentration either higher or lower than the

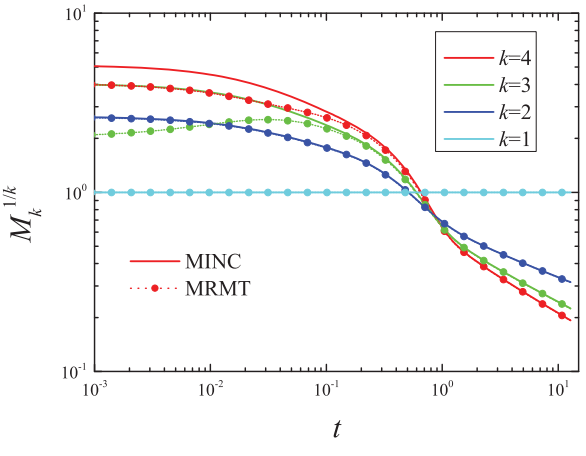

Figure 11. Temporal evolution of the first five moments of the concentration distribution $M_k^{1/k}$ for the layered case (n = 1) with nonuniform injection conditions along the immobile zone. Same parameters as in Figure 10.

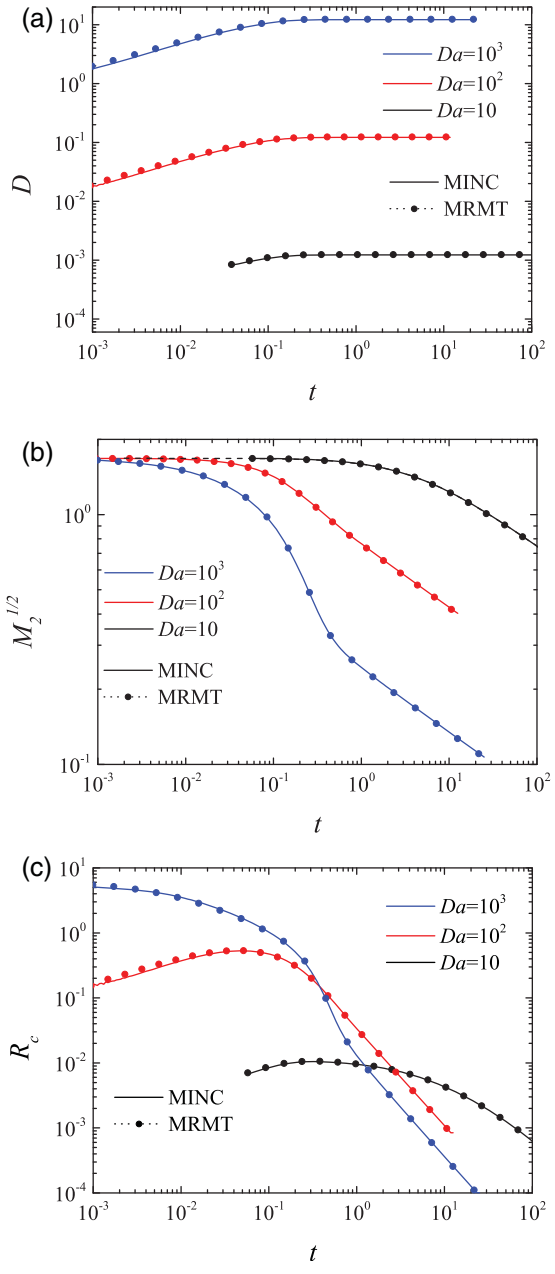

Figure 12. Temporal evolution of the (a) dispersion coefficient, (b) square root of the second moment of the concentration distribution, and (c) the reaction rate as functions of the Damköhler number (ratio of the characteristic diffusion time in the immobile zone to the characteristic advection time in the mobile zone). Parameters are synthesized in Table 2, column section 4.

other one. However, it is a severe limitation when considering that the transported species are directly chemical elements. The concept of immobile zone concentration should then be taken with great care and systematically assessed when modifying the initial conditions.

4.3. Influence of Immobile Porosity Structure on Reactivity

[51] The case of the nonuniform injection conditions shows that a more complex initial organization of the concentration field highlights the topological differences between the MRMT and MINC models (Figure 1) and that these differences can be nonnegligible as long as the concentration field retains the memory of the initial organization. Differences in reactivity might be even higher with more complex topological structures of the immobile zones. We have so far considered only two cases. Either all immobile zones are connected to the mobile zone, or the immobile zones (MRMT) are linearly connected between themselves (MINC). Inclusion dimensionality does not change the topology but the distribution of the volumes affected to the immobile zones. More complex topological structure may however occur in natural media. While, in fractured media, the observed wide-range distribution of the diffusion times [*Liu et al.*, 2004, 2007; *Zhou et al.*, 2007] has been related to the distribution of matrix-block sizes [*Haddad et al.*, 2012; *Kfoury et al.*, 2006; *Roubinet et al.*, 2010, 2012, 2013; *Zhan et al.*, 2009], it might also come from the topology of dead end and poorly linked fractures, which extension sharply increases from 2-D to 3-D [*de Dreuzy et al.*, 2001, 2012b]. Such secondary structures occur on a large range of scales from the fracture scale because of fracture aperture heterogeneities and from the

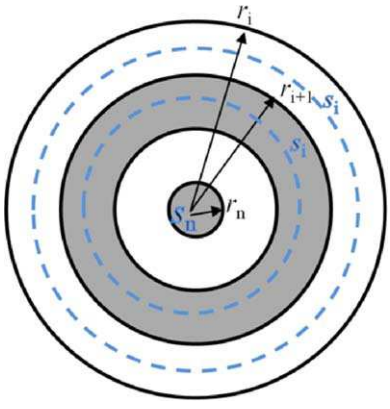

Figure 13. Sketch of the annuli and concentrations for cylindrical immobile zones ($n = 2$). The concentration s_i is defined at the middle of the two successive annuli r_i and r_{i+1}.

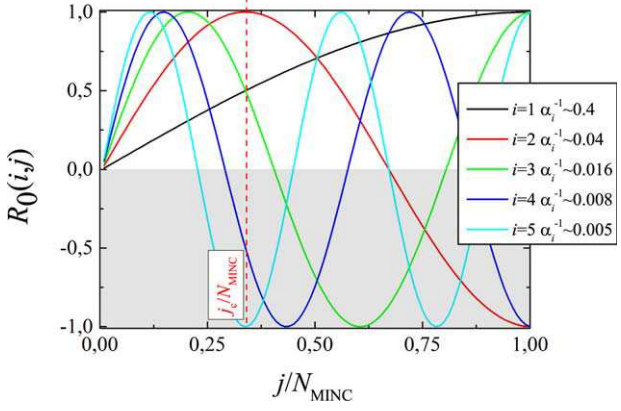

Figure 14. R_0(i, j) (equation (B9)) as a function of j/N_{MINC} for the five smallest MRMT rates (i = 1, . . ., 5).

complexity of the fracture gouge [*Andersson et al*., 2004; *Auradou et al*., 2006; *Brown et al*., 1998; *Méheust and Schmittbuhl*, 2001] to the network scale [*Davy et al*., 2006, 2010; *Odling*, 1997]. Multiple INteracting Continua result essentially from a discretization of the nonfractured part of the rock (matrix) according to the sole metric of the distance to the mobile zone [*Karimi-Fard et al*., 2006]. A topological characteristic might however be necessary for modeling reactive transport shifting the Multiple INteracting Continua framework (MINC) to a Structure INteracting Continua framework (SINC). Structure can be straightforwardly embedded in the developed formalism by simply modifying the matrix A of equation (12) characterizing the interaction between the immobile zones to include branching and dead ends parameters controlling the metric and topological organization of the immobile zones like what has classically been done for fractals or networks [*Barrat et al*., 2012; *Bouchaud and Georges*, 1990; *Havlin and Ben-Avraham*, 1987]. The range of possible topological structures may be further extended to those resulting from connectivity structures in porous media [*Le Goc et al*., 2009; *Renard and Allard*, 2012], or resulting from reactive transport processes like wormholes and dissolution patterns [*Andreani et al*., 2009; *Daccord et al*., 1993; *Fredd and Folger*, 1998; *Golfier et al*., 2002].

[52] Although incomplete, simplified interaction models like the Multi-Rate Mass Transfer (MRMT), the Multiple INteracting Continua (MINC), or the Structured INteracting Continua (SINC) are of interest as they propose an intermediary level of complexity to analyze nonlinear processes as mixing and the induced reactivity. On one hand, they maintain some structure in the model. On the other hand, they are not as complex as fully heterogeneous models for which analytical approximations still rely on some complex numerical closure assumptions [*Chiogna et al*., 2011; *de Dreuzy et al*., 2012a; *Jha et al*., 2011a, 2011b; *Kapoor and Kitanidis*, 1998; *Tennekes and Lumley*, 1972].

[53] While diffusion has a strong homogenization effect on transport processes and practically removes the details of the structures including most of the topological characteristics [*Haggerty and Gorelick*, 1995; *Villermaux*, 1987], chemical reactions coupled to diffusion may lead to significantly more localization and segregation as observed on the influence of concentration fluctuations [*de Anna et al*., 2011] and in geochemical self-organization, auto-catalytic reactions and where dimensionality has a critical influence [*Ortoleva*, 1994; *Pearson*, 1993; *Renard et al*., 1998]. Reactivity is, however, expected to differ from these pure diffusion-reaction processes because of the coupling induced by the mobile zone. Solute at evolving concentrations are constantly either brought up or removed from the immobile zone. If connections with the immobile zone are strong like in the MRMT model, the mobile zone will be likely more important than in more linear and ramified structures for which mobile/immobile interactions are limited to a single immobile zone. Interaction with the mobile zone is also expected to have more complex effects because of the strong organization of the velocity field induced by permeability heterogeneities [*Chiogna et al*., 2011; *Le Borgne et al*., 2007, 2008; *Luo and Cirpka*, 2008, 2011] that cannot be reduced to diffusion-like processes [*Becker and Shapiro*, 2000].

5. Conclusion

[54] We investigate numerically the influence of the immobile zone structure on mixing characteristics, concentration distribution, and reaction rate of a simple bimolecular reaction at chemical equilibrium in the framework of mobile/immobile models. The comparison relies on the MRMT and MINC immobile zone organizations both based on the diffusion in one-dimensional diffusive inclusions. In Multi-Rate Mass Transfer models (MRMT), all immobile zones are directly linked to the mobile zone, and this mobile zone is the only exchanger between the immobile zones (star connectivity). In Multiple INteracting Continua models (MINC), immobile zones are linked as a regular chain with a single element in relation with the immobile zone whatever the dimensionality of the immobile zone (chained connectivity). As both models derive from the same equation, they are equivalent in terms of transport in the mobile zone. Immobile zone concentrations in the MRMT model are a byproduct of the equivalence and are denominated "virtual concentrations" before checking their relevance to model real chemical concentrations. We use the simple bimolecular reaction at equilibrium as a typical example of chemical reactivity.

[55] We show that both MRMT and MINC models have the same concentration variance whatever the model parameters, dimensionality, and initial conditions. While their concentration variance strongly evolves with the model parameters and immobile zone dimensionality, they do not depend on the organization of the immobile zone, star connectivity in MRMT and chained connectivity in MINC. We confirm analytically this result for the flush of an n-dimensional immobile zone. When chemical reactivity is dominated by characteristics derived from the concentration variance (like the scalar dissipation rate), reactivity is independent of the structure of immobile porosity, and immobile zone "virtual concentrations" in the MRMT models can be handled as real chemical concentrations.

[56] However, the porosity structure has a critical influence on chemical reactivity when initial conditions induce more complex mixing patterns. It is especially the case for high initial concentration gradients in the immobile zone. Differences in higher moments of the immobile concentration distributions are amplified by the nonlinearity of the chemical reaction. Some of the immobile zone "virtual concentrations" in the MRMT model are negative to offset the direct connectivity of all immobile zones to the mobile zone. When high initial "virtual concentrations" are distant from the mobile zone, the immediate exchange with positive immobile zone concentrations is offset by exchanges with negative immobile zone "virtual concentrations" ensuring some delay of the concentration breakthrough to the mobile zone. Negative "virtual concentrations" may not be a fundamental problem for conservative components, which are linear combination of species concentrations. Yet they imply a severe limitation to MRMT models for the transport of real chemical concentrations. The concept of immobile zone concentration should then be taken with great care and systematically assessed when modifying the initial conditions.

[57] Strong immobile concentration gradients highlight the role of immobile porosity structure on chemical

reactivity and on the limits of the relevance of the MRMT to model chemical reactivity. Further evaluations are needed for more complex topological structures of the immobile zones and for complete chemical systems.

Appendix A: Mass and Interaction Matrix for the MRMT and MINC Models With Diffusion in Dimension *n*

[58] We discretize equations (9–11) according to a finite volume scheme for which the unknown concentrations S_i are taken at the middle between the annuli of radii r_i and r_{i+1} (Figure 13)

$$v_n\left(r_i^n - r_{i+1}^n\right)\frac{\partial S_i}{\partial t} = Q_{i+1} - Q_i \quad \text{for} \quad i=1,\ldots,N_{MINC}-1, \tag{A1}$$

where $r_1,\ldots,r_{N_{MINC}+1}$ is a concentric discretization starting at the interface between the mobile and immobile zones $r_1 = 1$ and ending at the immobile zone center $r_{N_{MINC}+1}=0$, v_n is the volume of the unit sphere in dimension n (v_n is equal to 1, π, and $4/3\pi$ for $n = 1$, 2, and 3) and the fluxes Q_i are given by

$$\begin{gathered} Q_1 = -a_n\frac{2r_1^{n-1}}{r_1 - r_2}(C - S_1) \\ Q_i = -a_n\frac{2r_i^{n-1}}{r_{i-1} - r_{i+1}}(S_{i-1} - S_i) \quad \text{for} \quad i=2...N_{MINC}-1 \\ Q_{N_{MINC}+1} = 0, \end{gathered} \tag{A2}$$

where a_1 is the surface of the unit sphere in dimension n (a_n is equal to 1, 2π, and 4π for $n = 1$, 2, and 3). The concentration c is considered homogeneous in the mobile zone at position x. Equation (9) is rewritten to integrate the continuity of solute flux at the mobile/immobile interface and modified to keep symmetrical expressions for the diffusive fluxes

$$\left(\frac{\sigma}{a_n r_1^{n-1}}\right)^{-1}\left(\frac{\partial C(x,t)}{\partial t} - L(C)\right) = Q_1, \tag{A3}$$

where σ is the ratio of the porous surface of the mobile/immobile interface per unit mobile volume [*Carrera et al.*, 1998] and L is the transport operator defined in equation (13). With the additional knowledge of the mean surface to volume ratio of the matrix blocks S_{im}/V_{im}, σ can straightforwardly be related to the porous volume ratio β of equation (2) by

$$\sigma = \frac{S_{im}}{V_{im}}\beta. \tag{A4}$$

[59] The surface to volume ratio in dimension n is $S_{im}/V_{im} = n/r_1$. The diagonal mass matrix defined by equation (12) is deduced with some rearrangement of the mobile equation (A3) to express A_{MINC} as a symmetrical matrix. As diffusion is a nondirectional process, A_{MINC} can in fact be expressed as a symmetrical matrix

$$\begin{gathered} M_{MINC}(1,1) = \frac{v_n r_1^n}{\beta} \\ M_{MINC}(i,i) = v_n\left(r_{i-1}^n - r_i^n\right) \quad \text{for} \quad i=2,\ \ldots,N_{MINC}+1, \end{gathered} \tag{A5}$$

where we also accounted for the shift of indices in the immobile zone. Note that $\frac{v_n r_1^n}{\beta}$ is simply the volume of the mobile zone expressed as a function of the capacity ratio β and of the characteristic volume of the immobile zone. The immobile to mobile porosity ratio is contained in β. Using (12) and (A1–A4), we deduce the interaction matrix

$$\begin{gathered} A_{MINC}(2,1) = 2a_n\frac{r_1^{n-1}}{r_1 - r_2} \\ A_{MINC}(1,2) = A_{MINC}(2,1) \\ A_{MINC}(1,1) = -A_{MINC}(1,2) \\ A_{MINC}(i-1,i) = 2a_n\frac{r_{i-1}^{n-1}}{r_{i-2} - r_i} \quad \text{for} \quad i=3,\ldots,N_{MINC} \\ A_{MINC}(i,i+1) = A_{MINC}(i-1,i) \quad \text{for} \quad i=3,\ldots,N_{MINC} \\ A_{MINC}(i,i) = -\left(A_{MINC}(i,i+1) + A_{MINC}(i,i-1)\right) \quad \text{for} \quad i=2,\ldots,N_{MINC}-1 \\ A_{MINC}(i,i) = -A_{MINC}(i,i-1) \quad \text{for} \quad i=N_{MINC}. \end{gathered} \tag{A6}$$

[60] A_{MINC} is a tri-diagonal matrix. All elements outside of the three central diagonals are equal to zero.

[61] Multi-Rate Mass Transfer models are expressed by equation (9) in the mobile zone and the following equation in the immobile zone

$$\frac{\partial S_i}{\partial t} = \alpha_i(C - S_i) \quad \text{for} \quad i=2,\ldots,N_{MRMT}+1. \tag{A7}$$

[62] The derivation of the Multi-Rate Mass Transfer model equivalent to the diffusion within an immobile zone of dimension n leads to the following mass and interaction matrices [*Carrera et al.*, 1998; *Haggerty and Gorelick*, 1995]

$$\begin{gathered} M_{MRMT}(1,1) = \frac{v_n r_1^n}{\beta} \\ M_{MRMT}(i,i) = V_N^n b_{i-1} \text{for} \quad i=2,,\ldots,N_{MRMT}+1 \end{gathered} \tag{A8}$$

and

$$\begin{cases} A_{MRMT}(1,i) = 2nV_N^n \\ A_{MRMT}(i,i) = -2n\ V_N^n \quad \text{for} \quad i=2,\ldots,N_{MRMT}+1 \\ A_{MRMT}(i,1) = 2nV_N^n \end{cases} \tag{A9}$$

$$A_{MRMT}(1,1) = -\sum_{i=2}^{N_{MRMT}+1} A(1,i),$$

where only the first N_{MRMT} elements of the infinite series have been kept

$$V_N^n = \frac{v_n r_1^n}{\sum_{i=1}^{N} b_i} \tag{A10}$$

and the exchange rate of the immobile porosity of α_i is denoted b_i. The series of α_i and b_i can directly be derived from *Haggerty and Gorelick* [1995, Table 1]

$$\begin{aligned} n=1 \;\; \alpha_i &= \frac{(2i-1)^2\pi^2}{4} \\ n=2 \;\; \alpha_i &= u_i^2 \\ n=3 \;\; \alpha_i &= i^2\pi^2 \end{aligned} \tag{A11}$$

with u_i the ith root of the zero-order Bessel function of the first kind and

$$b_i = \frac{2n}{\alpha_i}. \tag{A12}$$

[63] The normalization by the sum of b_i coefficients is required to enforce that the ratio of the immobile to mobile porous volumes be equal to β. The interaction matrix A_{MRMT} is an arrow-type of matrix with only nonzero elements in the first line, in the first column and in the diagonal expressing a star-shaped connectivity structure.

Appendix B: Relation Between Initial Immobile-Zone Concentrations in the Diffusive Flush of a 1-D Immobile Zone

[64] This appendix considers the simpler case of a 1-D diffusion with simplified initial and boundary conditions. In 1-D, the dimensionless diffusion equation is

$$\frac{\partial s}{\partial t} = \frac{\partial^2 s}{\partial y^2} \text{for } 0 \le y \le 1, \tag{B1}$$

where $s(y, t)$ is the concentration in the immobile zone at the distance 1-y from the mobile zone. Under more specific initial and boundary conditions, a fully analytical solution may also be derived using the method of separation of variables. Assuming $c(t) = 0$

$$s(y,t) = \sum_{i=1}^{\infty} \gamma_i \sin\left(\sqrt{\alpha_i} y\right) e^{-\alpha_i t} \tag{B2}$$

with

$$\gamma_i = 2\int_0^1 s_0(y) \sin\left(\sqrt{\alpha_i} y\right) dy. \tag{B3}$$

[65] Integrating over y leads to the classical expression of the MRMT model in 1-D. We derive the relation between the initial concentrations in the MRMT and MINC models from the general expressions (B2) and (B3). For MINC, we simply average the concentration along the immobile zone in N_{MINC} elements of equal dimension $1/N_{MINC}$

$$S_0^{MINC}(j) = N_{MINC} \int_{\frac{j-1}{N_{MINC}}}^{\frac{j}{N_{MINC}}} s_0(y)\, dy \tag{B4}$$

for $j = 1, \ldots, N_{MINC}$. We recall that lower and upper case concentrations stand, respectively, for continuous and integrated quantities. For MRMT, we express that the exchanges between mobile and immobile zones are equal to that in the diffusion solution and find

$$S_0^{MRMT}(i) = \frac{1}{2}\sqrt{\alpha_i}\gamma_i \tag{B5}$$

for $i = 0, \ldots, N_{MRMT}$, where γ_i is given by (B3). If we further assume that the initial concentration is discretized as in the MINC model, we can express from (B5) a relation between the initial concentrations in the MINC and MRMT models

$$S_0^{MRMT}(i) = 2\sin\left(\frac{\sqrt{\alpha_i}}{2N_{MINC}}\right) \sum_{j=1}^{N_{MINC}} \sin\left(\frac{\sqrt{\alpha_i}}{2N_{MINC}}(2j-1)\right) S_0^{MINC}(j), \tag{B6}$$

which can also be expressed in algebraic form

$$S_0^{MRMT} = 2D_0 R_0 S_0^{MINC} \tag{B7}$$

with D_0 the square diagonal matrix of size N_{MRMT}^2

$$D_0(i,j) = \sin\left(\frac{\sqrt{\alpha_i}}{2N_{MINC}}\right)\delta(i,j) \tag{B8}$$

[66] R_0 the full rectangular matrix N_{MRMT}. N_{MINC} of coefficients

$$R_0(i,j) = \sin\left(\frac{\sqrt{\alpha_i}}{2N_{MINC}}(2j-1)\right) \tag{B9}$$

and $S_0^{MRMT} = \left(s_0^{MRMT}(1), \ldots, s_0^{MRMT}(N_{MRMT})\right)^T$ and $S_0^{MINC} = \left(s_0^{MINC}(1), \ldots, s_0^{MINC}(N_{MINC})\right)^T$. Aside from the discretization and truncation errors in the MINC and MRMT models, the algebraic relation holds not only at the initial time but at all times and shows how the concentrations in the immobile zones are related in the MRMT and MINC frameworks.

[67] The diagonal matrix D_0 expresses a global weighting function of the discretization step of the MINC model while each element (i, j) of the matrix R_0 can be considered as the relative weight of the concentration at the position j/N_{MINC} in the MINC model to the concentration of the characteristic rate α_i in the MRMT model. As shown by Figure 14, the weight $R_0(i, j)$ strongly evolves with j/N_{MINC} and, apart from the smallest rate α_1 ($i = 1$), take both positive and negative values (in the white and gray parts of the graph, respectively). Depending on the initial concentrations in the MINC model, some of the initial concentrations in the MRMT model can be negative. The case of a uniform injected concentration in the MINC model is quite specific as it induces a uniform concentration in the MRMT model with all initial MRMT concentrations positive [*Haggerty and Gorelick*, 1995]. We can indeed show that $2D_0(i,i)\sum_{j=1}^{N_{MINC}} R_0(i,j)$ tends to 1 when N_{MINC} tends to infinity whatever the value of i. The uniform injection case gives also some indications on the relative contribution of the MINC zones to the MRMT transfer rates. For a given rate α_i of index i, only the first quarter period of $R(i, j)$ as a

function of j is nonzero as the remaining of the sum is performed over an integer number of half periods. The critical value of j below which the sum gives a nonzero contribution is denoted j_c (Figure 14) and is approximately equal to

$$\frac{j_c}{N_{MINC}} \approx \frac{1}{2i-1}. \tag{B10}$$

[68] For $i = 1$, the full immobile zone contributes positively to the first MRMT rate α_1, while, for $i = 2$, only the first third closest to the mobile zone contributes positively to the second MRMT rate α_2. For higher rates (smaller characteristic times), the positive contribution to the MRMT concerns always a smaller part of the immobile zone next to the mobile zone. Globally, the first transfer rate of the MRMT model is the sole rate that accounts positively for around the two-thirds of the immobile zone remote from the mobile zone. It is a large percentage that is reflected by the importance in volume of the first rate relatively to the other rates ($b_1 \sim 0.8$).

Appendix C: Second Moment of the Concentration Distribution in the Diffusive Flush of a 1-D Immobile Zone

[69] We start by computing the mean of the concentration squared in the MINC framework from its expression derived in Appendix B in the particular case of the same number of terms for the MINC and MRMT models $N_{MINC} = N_{MRMT}$. As the solution (B2) has been obtained using the method of separation of variables, we express it as

$$\int_{y=0}^{1} s^2(y,t)dy = \sum_{k=1}^{N_{MINC}} \sum_{i'=1}^{N_{MINC}} \gamma_i \gamma_{i'} e^{-(\alpha_i+\alpha_{i'})\bar{t}} \int_0^1 \sin\left(\sqrt{\alpha_i}y\right)\sin\left(\sqrt{\alpha_{i'}}y\right)dy \tag{C1}$$

which simplifies to

$$\int_{y=0}^{1} s^2(y,t)dy = \sum_{i=1}^{N_{MINC}} b_i \left(s_0^{MRMT}(k)e^{-\alpha_i t}\right)^2 \tag{C2}$$

by using (A11), (B5) and the orthogonality of the sine functions

$$\int_0^1 \sin\left(\sqrt{\alpha_i}y\right)\sin\left(\sqrt{\alpha_{i'}}y\right)dy = \frac{1}{2}\delta(i,i') \tag{C3}$$

[70] The right-hand side term of equation (C2) is precisely the solution of the MRMT model with an initial nonuniform concentration S_0^{MRMT}. The equality (C2) of the mean squared concentration directly derives from the orthogonality of the basis function used to express the analytical solution with the method of separation of variables. This argument does no longer hold for higher-order moments for which the product of more than three sine functions does not integrate necessarily to 0.

Appendix D: Flush of a 1-D Immobile Zone

[71] To get some additional insights into the conservation of the concentration variance, we consider the simpler problem of the flush by diffusion of 1-D immobile zone corresponding to equations (3), (5), and (6) with uniform initial conditions

$$s(r, t=0) = 1. \tag{D1}$$

[72] The concentration in the mobile zone is set to zero at all times. Solutions to this simpler problem are fully analytical both for the diffusion problem (Appendix B, equations (B2) and (B3)) and for the MRMT model

$$s_i(t) = \exp\left(-\alpha_i t\right) \tag{D2}$$

for $i = 1, \ldots, \infty$ and where the coefficients α_i are given by equation (A11). Both solutions are expressed as infinite series that we truncate at a large enough index (200) so that the truncation error can be neglected. Parameters are otherwise identical to those used in the previous section. We check that the total variation of masses in the immobile zone are equal for the MRMT and diffusion models (Figure 7a). The $M_2^{1/2}$ values are also equal between both models (Figure 7b, black lines). This equality can be demonstrated analytically in this specific 1-D diffusion case whatever the initial conditions (Appendix C). The equality fundamentally comes from the orthogonality of the family of functions used to construct the solution within the variable separation method. The higher-order integrals $M_k^{1/k}$ however differ (Figure 7b, colored lines). The full evolution of $M_k^{1/k}$ with k is shown in Figure 8 for k ranging from 0.1 to 3.5. It shows that $M_k^{1/k}$ values are equal between both models for $k = 1$ and $k = 2$. Between 1 and 2, $M_k^{1/k}$ remain very similar while they slightly differ for lower and higher k values. As the moments only slightly differ, the distributions of concentration remain close between the diffusion and the MRMT models.

[73] Concerning now the differences between the distributions, the higher differences occur for the lower and higher values of the order k, which are more sensitive to the extreme of the distribution. In fact, the maximum concentrations differ and their difference can reach 25% (Figure 7c). They remain higher in the diffusion model than in the MRMT model as, at early times, they are away from the mobile zone and unaffected by the evolution of its concentration. In the MRMT model, however, the mobile/immobile exchanges affect all concentrations including their maximum at once. Minimal concentrations have also higher probabilities in the diffusion model than in MRMT (Figure 8). The concentration distribution is wider in the diffusion model than in MRMT. The stronger importance of intermediary concentrations in the MRMT model fundamentally comes from the extreme dominance of the concentrations of the lowest rates with the highest porosity ratios (Table 1). The concentration distribution dominated by these few discrete values is narrower with smaller probability of occurrence of its extremes. To maintain an equivalent exchange between mobile and immobile zones, MRMT thus includes a compensation mechanism where

less smaller concentrations are compensated by less larger concentrations.

[74] **Acknowledgments.** The European Union is acknowledged for its funding through the Marie-Curie fellowship PIEF-GA-2009–251710 and the ANR through its project H2MNO4 under ANR-12-MONU-0012-01. The INRA-INRIA "VITELBIO" is also acknowledged to have supported the collaboration between the first, second, and fourth authors. We thank Tim Ginn and Ahmed Ali for their careful review and relevant contribution to the paper and Daniel Fernandez-Garcia for his editorial work.

References

Andersson, P., J. Byegård, E.-L. Tullborg, T. Doe, J. Hermanson, and A. Winberg (2004), In situ tracer tests to determine retention properties of a block scale fracture network in granitic rock at the Aspo Hard Rock Laboratory, Sweden, *J. Contam. Hydrol.*, *70*(3–4), 271–297.

Andreani, M., L. Luquot, P. Gouze, M. Godard, E. Hoisé, and B. Gibert (2009), Experimental study of carbon sequestration reactions controlled by the percolation of CO_2-rich brine through peridotites, *Environ. Sci. Technol.*, *43*(4), 1226–1231.

Aquilina, L., and J.-R. de Dreuzy (2011), Relationship of present saline fluid with paleomigration of basinal brines at the basement/sediment interface (Southeast basin of France), *Appl. Geochem.*, *26*(12), 1933–1945.

Aquilina, L., P. Boulvais, and J.-R. Mossmann (2011), Fluid migration at the basement/sediment interface along the margin of the Southeast basin (France): Implications for Pb-Zn ore formation, *Miner. Deposita*, *46*(8), 959–979, doi:10.1007/s00126-011-0360-9.

Auradou, H., G. Drazer, A. Boschan, J. P. Hulin, and J. Koplik (2006), Flow channeling in a single fracture induced by shear displacement, *Geothermics*, *35*(5–6), 576–588.

Barrat, A., M. Barthélemy, and A. Vespignani (2012), *Dynamical Processes on Complex Networks*, Cambridge Univ. Press, Cambridge, U. K.

Başağaoğlu, H., B. J. McCoy, T. R. Ginn, F. J. Loge, and J. P. Dietrich (2002), A diffusion limited sorption kinetics model with polydispersed particles of distinct sizes and shapes, *Adv. Water Resour.*, *25*(7), 755–772.

Becker, M. W., and A. M. Shapiro (2000), Tracer transport in fractured crystalline rock: Evidence of nondiffusive breakthrough tailing, *Water Resour. Res.*, *36*(7), 1677–1686.

Benson, D. A., S. W. Wheatcraft, and M. M. Meerschaert (2000), Application of a fractional advection-dispersion equation, *Water Resour. Res.*, *36*(6), 1403–1412.

Berkowitz, B., A. Cortis, M. Dentz, and H. Scher (2006), Modeling non-Fickian transport in geological formations as a continuous time random walk, *Rev. Geophys.*, *44*, RG2003, doi:10.1029/2005RG000178.

Bouchaud, J.-P., and A. Georges (1990), Anomalous diffusion in disordered media: Statistical mechanisms, models and physical applications, *Phys. Rep.*, *195*(4–5), 127–293.

Brown, S., A. Caprihan, and R. Hardy (1998), Experimental observation of fluid flow channels in a single fracture, *J. Geophy. Res.*, *103*(B3), 5125–5132.

Carrera, J., X. Sanchez-Vila, I. Benet, A. Medina, G. Galarza, and J. Guimera (1998), On matrix diffusion: Formulations, solution methods and qualitative effects, *Hydrogeol. J.*, *6*(1), 178–190.

Charlton, S. R., and D. L. Parkhurst (2011), Modules based on the geochemical model PHREEQC for use in scripting and programming languages, *Comput. Geosci.*, *37*(10), 1653–1663.

Chiogna, G., O. A. Cirpka, P. Grathwohl, and M. Rolle (2011), Transverse mixing of conservative and reactive tracers in porous media: Quantification through the concepts of flux-related and critical dilution indices, *Water Resour. Res.*, *47*, W02505, doi:10.1029/2010WR009608.

Daccord, G., O. Lietard, and R. Lenormand (1993), Chemical dissolution of a porous-medium by a reactive fluid. 1. Model for the wormholing phenomenon, *Chem. Eng. Sci.*, *48*(1), 169–178.

Daus, A. D., E. O. Frind, and E. A. Sudicky (1985), Comparative error analysis in finite-element formulations of the advection-dispersion equation, *Adv. Water Resour.*, *8*(2), 86–95.

Davy, P., O. Bour, J.-R. de Dreuzy, and C. Darcel (2006), Flow in multiscale fractal fracture networks, *Geol. Soc. Spec. Publ.*, *261*(1), 31–45.

Davy, P., R. Le Goc, C. Darcel, O. Bour, J. R. de Dreuzy, and R. Munier (2010), A likely universal model of fracture scaling and its consequence for crustal hydromechanics, *J. Geophys. Res.*, *115*, B10411, doi:10.1029/2009JB007043.

de Anna, P., T. Le Borgne, M. Dentz, D. Bolster, and P. Davy (2011), Anomalous kinetics in diffusion limited reactions linked to non-Gaussian concentration probability distribution function, *J. Chem. Phys.*, *135*(17), 174104.

de Dreuzy, J.-R., P. Davy, and O. Bour (2001), Hydraulic properties of two-dimensional random fracture networks following a power law length distribution: 1. Effective connectivity, *Water Resour. Res.*, *37*(8), 2065–2078.

de Dreuzy, J.-R., J. Carrera, M. Dentz, and T. Le Borgne (2012a), Time evolution of mixing in heterogeneous porous media, *Water Resour. Res.*, *48*, W06511, doi:10.1029/2011WR011360.

de Dreuzy, J.-R., Y. Méheust, and G. Pichot (2012b), Influence of fracture scale heterogeneity on the flow properties of three-dimensional Discrete Fracture Networks (DFN), *J. Geophys. Res.*, *117*, B11207, doi:10.1029/2012JB009461.

Dentz, M., and B. Berkowitz (2003), Transport behavior of a passive solute in continuous time random walks and multirate mass transfer, *Water Resour. Res.*, *39*(5), 1111, doi:10.1029/2001WR001163.

de Simoni, M., J. Carrera, X. Sánchez-Vila, and A. Guadagnini (2005), A procedure for the solution of multicomponent reactive transport problems, *Water Resour. Res.*, *41*, W11410, doi:10.1029/2005WR004056.

Donado, L. D., X. Sanchez-Vila, M. Dentz, J. Carrera, and D. Bolster (2009), Multicomponent reactive transport in multicontinuum media, *Water Resour. Res.*, *45*, W11402, doi:10.1029/2008WR006823.

Fernàndez-Garcia, D., G. Llerar-Meza, and J. J. Gómez-Hernández (2009), Upscaling transport with mass transfer models: Mean behavior and propagation of uncertainty, *Water Resour. Res.*, *45*, W10411, doi:10.1029/2009WR007764.

Fourcade, S., L. Trotignon, P. Boulvais, I. Techer, M. Elie, D. Vandamme, E. Salameh, and H. Khoury (2007), Cementation of kerogen-rich marls by alkaline fluids released during weathering of thermally metamorphosed marly sediments. Part I: Isotopic (C,O) study of the Khushaym Matruk natural analogue (central Jordan), *Appl. Geochem.*, *22*(7), 1293–1310.

Fredd, C. N., and H. S. Folger (1998), Alternative stimulation fluids and their impact on carbonate acidizing, *Soc. Pet. Eng. J.*, *13*(34), 34–41.

Ginn, T. R. (2009), Generalization of the multirate basis for time convolution to unequal forward and reverse rates and connection to reactions with memory, *Water Resour. Res.*, *45*, W12419, doi:10.1029/2009WR008320.

Glassley, W. E., A. M. Simmonsb, and J. R. Kercher (2002), Mineralogical heterogeneity in fractured, porous media and its representation in reactive transport models, *Appl. Geochem.*, *17*(6), 699–708.

Godsil, C., and G. F. Royle (2001), Algebraic Graph Theory, Springer, New York.

Golfier, F., C. Zarcone, B. Bazin, R. Lenormand, D. Lasseux, and M. Quintard (2002), On the ability of a Darcy-scale model to capture wormhole formation during the dissolution of a porous medium, *J. Fluid Mech.*, *457*, 213–254.

Golfier, F., M. Quintard, F. Cherblanc, B. A. Zinn, and B. D. Wood (2007), Comparison of theory and experiment for solute transport in highlyheterogeneous porous medium, *Adv. Water Resour.*, *30*(11), 2235–2261.

Gouze, P., Y. Melean, T. Le Borgne, M. Dentz, and J. Carrera (2008), Non-Fickian dispersion in porous media explained by heterogeneous microscale matrix diffusion, *Water Resour. Res.*, *44*, W11416, doi:10.1029/2007WR006690.

Gramling, C. M., C. F. Harvey, and L. C. Meigs (2002), Reactive transport in porous media: A comparison of model prediction with laboratory visualization, *Environ. Sci. Technol.*, *36*(11), 2508–2514.

Grisak, G. E., and J. F. Pickens (1980), Solute transport through fractured media. 1. The effect of matrix diffusion, *Water Resour. Res.*, *16*(4), 719–730.

Haddad, A. S., H. Hassanzadeh, and J. Abedi (2012), Advective-diffusive mass transfer in fractured porous media with variable rock matrix block size, *J. Contam. Hydrol.*, *133*, 94–107.

Haggerty, R., and S. M. Gorelick (1995), Multiple-rate mass transfer for modeling diffusion and surface reactions in media with pore-scale heterogeneity, *Water Resour. Res.*, *31*(10), 2383–2400.

Haggerty, R., S. A. McKenna, and L. C. Meigs (2000), On the late-time behavior of tracer test breakthrough curves, *Water Resour. Res.*, *36*(12), 3467–3479.

Haggerty, R., C. F. Harvey, C. Freiherr von Schwerin, and L. C. Meigs (2004), What controls the apparent timescale of solute mass transfer in aquifers and soils? A comparison of experimental results, *Water Resour. Res.*, *40*, W01510, doi:10.1029/2002WR001716.

Haidar, I., A. Rapaport, and F. Gérard (2011), Effects of spatial structure and diffusion on the performances of the chemostat, *Math. Biosci. Eng.*, *8*(4), 953–971.

Havlin, S., and D. Ben-Avraham (1987), Diffusion in disordered media, *Adv. Phys.*, *36*(6), 695–798.

Hochstetler, D. L., M. Rolle, G. Chiogna, C. M. Haberer, P. Grathwohl, and P. K. Kitanidis (2013), Effects of compound-specific transverse mixing on steady-state reactive plumes: Insights from pore-scale simulations and Darcy-scale experiments, *Adv. Water Resour.*, *54*, 1–10.

Jha, B., L. Cueto-Felgueroso, and R. Juanes (2011a), Fluid mixing from viscous fingering, *Phys. Rev. Lett.*, *106*(19), 194–502.

Jha, B., L. Cueto-Felgueroso, and R. Juanes (2011b), Quantifying mixing in viscously unstable porous media flows, *Phys. Rev. A*, *84*(6 Pt 2), 066312.

Kapoor, V., and P. K. Kitanidis (1998), Concentration fluctuations and dilution in aquifers, *Water Resour. Res.*, *34*(5), 1181–1193.

Karimi-Fard, M., B. Gong, and L. J. Durlofsky (2006), Generation of coarse-scale continuum flow models from detailed fracture characterizations, *Water Resour. Res.*, *42*, W10423, doi:10.1029/2006WR005015.

Kfoury, M., R. Ababou, B. Noetinger, and M. Quintard (2006), Upscaling fractured heterogeneous media: Permeability and mass exchange coefficient, *J. Appl. Mech.*, *73*(1), 41–46.

LeBlanc, D. R., S. P. Garabedian, K. M. Hess, L. W. Gelhar, R. D. Quadri, K. G. Stollenwerk, and W. W. Wood (1991), Large-scale natural gradient tracer test in sand and gravel, Cape Cod, Massachusetts, 1. Experimental design and observed tracer movement, *Water Resour. Res.*, *27*(5), 895–910.

Le Borgne, T., J.-R. de Dreuzy, P. Davy, and O. Bour (2007), Characterization of the velocity field organization in heterogeneous media by conditional correlations, *Water Resour. Res.*, *43*, W02419, doi:10.1029/2006WR004875.

Le Borgne, T., M. Dentz, and J. Carrera (2008), Spatial Markov processes for modeling Lagrangian particle dynamics in heterogeneous porous media, *Phys. Rev. A*, *78*(2 Pt 2), 9.

Le Borgne, T., M. Dentz, D. Bolsterc, J. Carrera, J.-R. de Dreuzy, and P. Davy (2010), Non-Fickian mixing: Temporal evolution of the scalar dissipation rate in heterogeneous porous media, *Adv. Water Resour.*, *33*(12), 1468–1475.

Le Goc, R., J.-R. de Dreuzy, and P. Davy (2009), Statistical characteristics of flow as indicators of channeling in heterogeneous porous and fractured media, *Adv. Water Resour.*, *33*(3), 257–269.

Li, L., H. Zhoua, and J. J. Gómez-Hernández (2011), Transport upscaling using multi-rate mass transfer in three-dimensional highly heterogeneous porous media, *Adv. Water Resour.*, *34*(4), 478–489.

Liu, H. H., G. S. Bodvarsson, and G. Zhang (2004), Scale dependency of the effective matrix diffusion coefficient, *Vadose Zone J.*, *3*(1), 312–315.

Liu, H. H., Y. Q. Zhang, Q. Zhou, and F. J. Molz (2007), An interpretation of potential scale dependence of the effective matrix diffusion coefficient, *J. Contam. Hydrol.*, *90*(1–2), 41–57.

Luo, J., and O. A. Cirpka (2008), Traveltime-based descriptions of transport and mixing in heterogeneous domains, *Water Resour. Res.*, *44*, W09407, doi:10.1029/2007WR006035.

Luo, J., and O. A. Cirpka (2011), How well do mean breakthrough curves predict mixing-controlled reactive transport?, *Water Resour. Res.*, *47*, W02520, doi:10.1029/2010WR009461.

Magnico, P., C. Leroy, J. P. Bouchaud, C. Gauthier, and J. P. Hulin (1993), Tracer dispersion in porous media with a double porosity, *Phys. Fluids A*, *5*(1), 46–57.

Maloszewski, P., and A. Zuber (1985), On the theory of tracer experiments in fissured rocks with a porous matrix, *J. Hydrol.*, *79*(3–4), 333–358.

McKenna, S. A., L. C. Meigs, and R. Haggerty (2001), Tracer tests in a fractured dolomite 3. Double-porosity, multiple-rate mass transfer processes in convergent flow tracer tests, *Water Resour. Res.*, *37*(5), 1143–1154.

Méheust, Y., and J. Schmittbuhl (2001), Geometrical heterogeneities and permeability anisotropy of rough fractures, *J. Geophy. Res.*, *106*(B2), 2089–2102.

Neretnieks, I. (1980), Diffusion in the rock matrix: An important factor in radionucleside retardation?, *J. Geophy. Res.*, *85*(B8), 4379–4397.

Neuman, S. P., and D. M. Tartakovsky (2009), Perspective on theories of non-Fickian transport in heterogeneous media, *Adv. Water Resour.*, *32*(5), 670–680.

Odling, N. E. (1997), Scaling and connectivity of joint systems in sandstones from western Norway, *J. Struct. Geol.*, *19*(10), 1257–1271.

Ortoleva, P. J. (1994), *Geochemical Self-Organization*, Oxford Univ. Press, Oxford, U. K.

Parkhurst, D. L., and C. A. J. Appelo (1999), User's guide to PHREEQC (version 2)—A computer program for speciation, batch-reaction, one-dimensional transport, and inverse geochemical calculations, U.S. Geol. Surv. Water Resour. Invest. Rep., 99–4259. 321 p.

Pearson, J. E. (1993), Complex patterns in a simple system, *Science*, *261*(5118), 189–192.

Pruess, K. (1992), *Brief Guide to the MINC—Method for Modeling Flow and Transport in Fractured Media*, Lawrence Berkeley Natl. Lab., Earth Sci. Div., Berkeley, Calif.

Pruess, K., and T. N. Narasimhan (1985), A practical method for modeling fluid and heat-flow in fractured porous-media, *Soc. Pet. Eng. J.*, *25*(1), 14–26.

Rao, P. S. C., D. E. Rolston, R. E. Jessup, and J. M. Davidson (1980), Solute transport in aggregated porous-media—Theoretical and experimental evaluation, *Soil Sci. Soc. Am. J.*, *44*(6), 1139–1146.

Renard, F., J.-P. Gratier, P. Ortoleva, E. Brosse, and B. Bazin (1998), Self-organization during reactive fluid flow in a porous medium, *Geophys. Res. Lett.*, *25*(3), 385–388.

Renard, P., and D. Allard (2012), Connectivity metrics for subsurface flow and transport, *Adv. Water Resour* 168–196.

Roubinet, D., H.-H. Liu, and J.-R. de Dreuzy (2010), A new particle-tracking approach to simulating transport in heterogeneous fractured porous media, *Water Resour. Res.*, *46*, W11507, doi:10.1029/2010WR009371.

Roubinet, D., J.-R. de Dreuzy, and D. M. Tartakovsky (2012), Semi-analytical solutions for solute transport and exchange in fractured porous media, *Water Resour. Res.*, *48*, W01542, doi:10.1029/2011WR011168.

Roubinet, D., J.-R. de Dreuzy, and D. M. Tartakovsky (2013), Particle-tracking simulations of anomalous transport in hierarchically fractured rocks, *Comput. Geosci.*, *50*(0), 52–58.

Rubin, J. (1983), Transport of reacting solutes in porous-media—Relation between mathematical nature of problem formulation and chemical nature of reactions, *Water Resour. Res.*, *19*(5), 1231–1252.

Shapiro, A. (2001), Effective matrix diffusion in kilometer-scale transport in fractured crystalline rock, *Water Resour. Res.*, *37*(3), 507–522.

Sudicky, E. A. (1986), A natural gradient experiment on solute transport in a sand aquifer: Spatial variability of hydraulic conductivity and its role in the dispersion process, *Water Resour. Res.*, *22*(13), 2069–2082.

Sudicky, E. A., and E. O. Frind (1982), Contaminant transport in fractured porous-media—Analytical solutions for a system of parallel fractures, *Water Resour. Res.*, *18*(6), 1634–1642.

Tang, D. H., E. O. Frind, and E. A. Sudicky (1981), Contaminant transport in fractured porous-media—Analytical solution for a single fracture, *Water Resour. Res.*, *17*(3), 555–564.

Techer, I., D. Bartier, Ph. Boulvais, E. Tinseau, K. Suchorski, J. Cabrera, and A. Dauzères (2012), Tracing interactions between natural argillites and hyper-alkaline fluids from engineered cement paste and concrete: Chemical and isotopic monitoring of a 15-years old deep-disposal analogue, *Appl. Geochem.*, *27*(7), 1384–1402.

Tennekes, H., and J. L. Lumley (1972), *A First Course in Turbulence*, MIT Press, Cambridge, Mass.

Villermaux, J. (1987), Chemical-engineering approach to dynamic modeling of linear chromatography—A flexible method for representing complex phenomena from simple concepts, *J. Chromatogr.*, *406*, 11–26.

Willmann, M., J. Carrera, and X. Sánchez-Vila (2008), Transport upscaling in heterogeneous aquifers: What physical parameters control memory functions?, *Water Resour. Res.*, *44*, W12437, doi:10.1029/2007WR006531.

Willmann, M., J. Carrera, X. Sanchez-Vila, O. Silva, and M. Dentz (2010), Coupling of mass transfer and reactive transport for nonlinear reactions in heterogeneous media, *Water Resour. Res.*, *46*, W07512, doi:10.1029/2009WR007739.

Wu, S. C., and P. M. Gschwend (1986), Sorption kinetics of hydrophobic organic-compounds to natural sediments and soils, *Environ. Sci. Technol.*, *20*(7), 717–725.

Wu, Y.-S., and K. Pruess (2000), Numerical simulation of non-isothermal multiphase tracer transport in heterogeneous fractured porous media, *Adv. Water Resour.*, *23*(7), 699–723.

Wu, Y. S., H. H. Liu, and G. S. Bodvarsson (2004), A triple-continuum approach for modeling flow and transport processes in fractured rock, *J. Contam. Hydrol.*, *73*(1–4), 145–179.

Zhan, H. B., Z. Wen, G. Huang, and D. Sun (2009), Analytical solution of two-dimensional solute transport in an aquifer-aquitard system, *J. Contam. Hydrol.*, *107*(3–4), 162–174.

Zhou, Q. L., H. H. Liu, F. J. Molz, Y. Zhang, and G. S. Bodvarsson (2007), Field-scale effective matrix diffusion coefficient for fractured rock: Results from literature survey, *J. Contam. Hydrol.*, *93*(1–4), 161–187.

Zinn, B., L. C. Meigs, C. F. Harvey, R. Haggerty, W. J. Peplinski, and C. F. von Schwerin (2004), Experimental visualization of solute transport and mass transfer processes in two-dimensional conductivity fields with connected regions of high conductivity, *Environ. Sci. Technol.*, *38*(14), 3916–3926.